Inorganic Chemistry

pubs.acs.org/IC Article

In Situ Bioconjugation of a Maleimide-Functionalized Ruthenium-Based Photosensitizer to Albumin for Photodynamic Therapy

Robin Vinck,*,# Orsolya Dömötör,# Johannes Karges, Marta Jakubaszek, Johanne Seguin, Mickaël Tharaud, Vincent Guérineau, Kevin Cariou, Nathalie Mignet, Éva A. Enyedy, and Gilles Gasser*

Cite This: *Inorg. Chem.* 2023, 62, 15510−15526 Read Online

ACCESS | Metrics & More | Article Recommendations | Supporting Information

ABSTRACT: Maleimide-containing prodrugs can quickly and selectively react with circulating serum albumin following their injection in the bloodstream. The drug−albumin complex then benefits from longer blood circulation times and better tumor accumulation. Herein, we have applied this strategy to a previously reported highly phototoxic Ru polypyridyl complex-based photosensitizer to increase its accumulation at the tumor, reduce off-target cytotoxicity, and therefore improve its pharmacological profile. Specifically, two complexes were synthesized bearing a maleimide group: one complex with the maleimide directly incorporated into the bipyridyl ligand, and the other has a hydrophilic linker between the ligand and the maleimide group. Their interaction with albumin was studied in-depth, revealing their ability to efficiently bind both covalently and noncovalently to the plasma protein. A crucial finding is that the maleimide-functionalized complexes exhibited significantly lower cytotoxicity in noncancerous cells under dark conditions compared to the nonfunctionalized complex, which is a highly desirable property for a photosensitizer. The binding to albumin also led to a decrease in the phototoxicity of the Ru bioconjugates in comparison to the nonfunctionalized complex, probably due to a decreased cellular uptake. Unfortunately, this decrease in phototoxicity was not compensated by a dramatic increase in tumor accumulation, as was demonstrated in a tumor-bearing mouse model using inductively coupled plasma mass spectrometry (ICP-MS) studies. Consequently, this study provides valuable insight into the future design of *in situ* albumin-binding complexes for photodynamic therapy in order to maximize their effectiveness and realize their full potential.

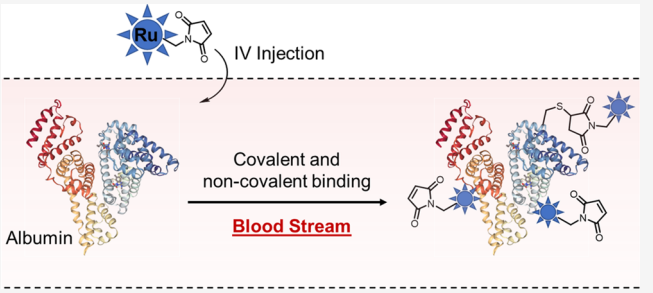

INTRODUCTION

In the past few years, photodynamic therapy (PDT) has gained growing interest in the fight against cancer. This approved medical technique involves the use of a photosensitizer (PS) and light in order to induce cellular damage in tumors in a spatially and temporally controlled manner.[1−4]

Typical PDT procedures start with local or systemic administration of the PS, followed after a certain time by local light irradiation of the targeted tissues. Light-mediated excitation of the PS leads to the generation of reactive oxygen species (ROS) and/or singlet oxygen ($^1O_2$), following a type I or type II mechanism, respectively, which are responsible for local cellular damage.[5]

Most clinically applied PSs are based on tetrapyrrolic scaffolds. First-generation PSs (*i.e.*, Photofrin and hematoporphyrin derivatives) are a mixture of several chemical entities. They have often been associated with slow elimination rates, leading to extended photosensitivity in patients, low aqueous solubility, photodegradation, tedious synthetic procedures, and lack of selectivity toward diseased tissues. Some of these drawbacks have been addressed to yield second-generation PSs (*e.g.*, Photosens, Foscan, Laserphyrin, Redaporphin, Photogem, Radachlorin, Purlytin, Lutrin, TOOKAD soluble) with better-defined structures, improved aqueous solubility, longer absorption wavelengths, and reduced skin sensitization. However, these second-generation porphyrin-based compounds are still far from the ideal of a perfect PS since only a few combine all of the aforementioned advantages.[2,4,6−8]

Among non-porphyrin PSs, the use of ruthenium(II) (Ru(II)) polypyridyl complexes has recently received much interest thanks to their simple synthesis, chemical stability, good $^1O_2$ production yields, and generally good aqueous solubility.[9−18] Notably, TLD-1433 is currently involved in a phase II clinical trial for patients with bladder cancer.[19,20] However, these Ru(II)-based PSs are known to poorly absorb light in the biological spectral window (600−900 nm).[8,21] This

Received: June 16, 2023
Published: September 14, 2023

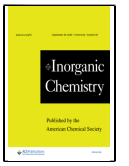

https://doi.org/10.1021/acs.inorgchem.3c01984
Inorg. Chem. 2023, 62, 15510−15526

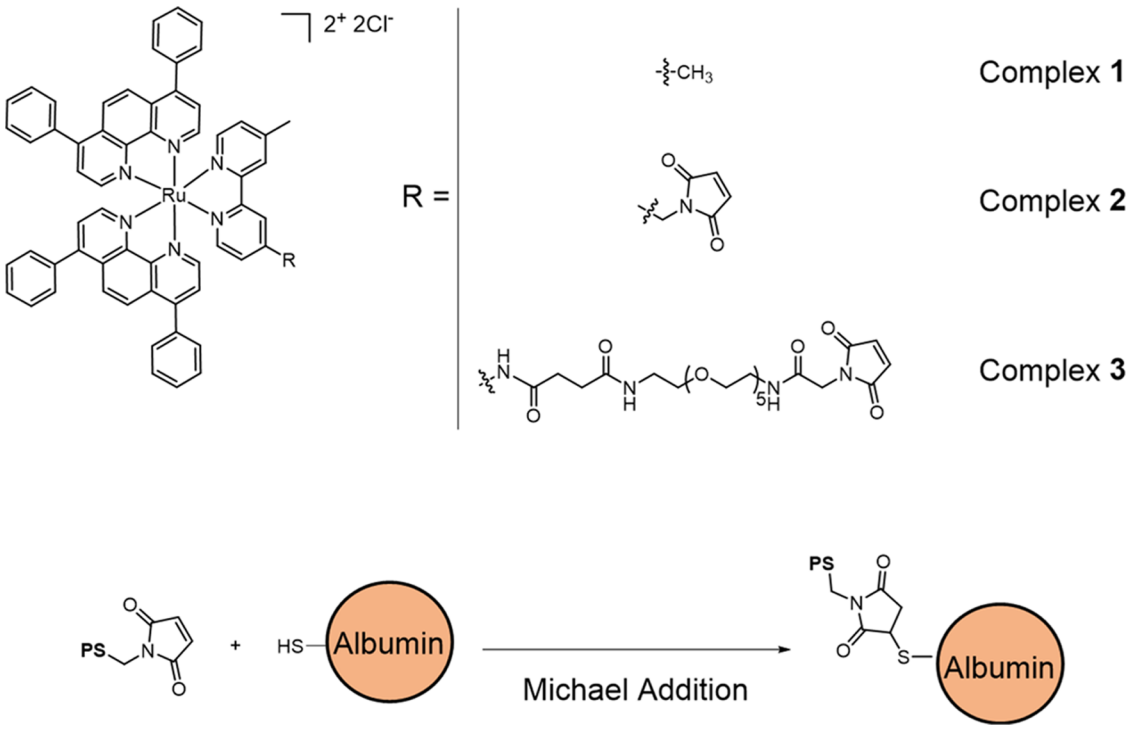

Figure 1. Chemical structures of the Ru(II) complexes studied in this work and putative scheme of a reaction of a maleimide-functionalized PS with the thiol group of cysteine-34 (Cys-34) of albumin.

feature prevents the treatment of tumors located deeply in the tissues or of large tumors.[22]

To address this drawback, we recently reported the density functional theory (DFT)-guided design and *in vitro* study of new Ru(II) polypyridyl complexes absorbing at longer wavelengths.[23] One of these compounds, namely, [**Ru(bphen)$_2$dmbipy**][**PF$_6$**]$_2$ (bphen = 4,7-diphenyl-1,10-phenanthroline, dmbipy = 4,4′-dimethyl-2,2′-bipyridine, Figure 1), which has previously been described by others for its cytotoxic properties,[24] showed a great PDT potential on various cancer cell lines in a two-dimensional (2D) cell monolayer model as well as in a three-dimensional (3D) HeLa multicellular tumor spheroid (MCTS) model. In contrast to the majority of published Ru(II) polypyridyl complexes, this compound was able to exert a phototoxic effect upon irradiation up to 595 nm, which lies at the frontier of the biological spectral window. In addition, [**Ru(bphen)$_2$dmbipy**][**PF$_6$**]$_2$ displays little photobleaching and good stability in human plasma.

PDT features a spatial and temporal control of the therapeutic effect, which intrinsically provides PDT with a first level of selectivity toward diseased tissues. However, to improve its therapeutic potential, PDT could benefit from a second level of selectivity by directly targeting the tumor.[25] Over the years, many strategies have been developed to increase the selectivity of chemotherapeutics toward cancer cells, either through active or passive targeting.[26−29] Some active targeting strategies have already been applied to Ru(II)-based PSs, including conjugation of the complex to aptamers,[30] antibodies and nanobodies,[29,31,32] oligonucleotides,[33,34] bombesin,[35−37] biotin,[33,38−41] folic acid,[42] somatostatin,[43] glucose,[44] mannose,[45] tamoxifen,[46] cobalamin,[47] taurine,[48] or transferrin.[34,49,50] Passive targeting strategies exploiting the enhanced permeation and retention (EPR) effect have also been explored through encapsulation or conjugation methods using polymers,[38,51−58] liposomes,[59,60] carbon nanotubes and graphene oxide,[61−63] inorganic materials,[34,42,64−72] or proteins.[71,73,74] It is worth noting that a substantial proportion of these studies combine both active and passive targeting to further enhance PS tumor selectivity.

Among these targeting approaches, the conjugation or binding of the PS to endogenous blood plasma proteins, and more particularly albumin, seems especially attractive to increase its blood residence time and promote its accumulation specifically within tumors.[75,76] Albumin is the most abundant plasma protein with a concentration of 35−50 g/L of human plasma.[77] This protein has been described to accumulate in tumors through the EPR effect[78−80] and also through a gp60 and caveolin-1-mediated transcytosis, promoting its extravasation from the blood circulation to the diseased tissues.[81,82] Several attempts to conjugate chemotherapeutic drugs to albumin in order to increase their tumor accumulation resulted in the clinical success of Abraxane, a now-marketed paclitaxel formulation with enhanced efficacy and safety compared to the classical formulation.[83−85] While albumin was predominantly investigated as a therapeutic carrier for purely organic drugs, there is a growing interest in exploring its potential for anticancer metal complexes.[86−90]

In particular, this strategy has already been successfully employed in the case of Ru(II)-based PSs. Shi et al. reported the elaboration of a nanocarrier based on lanthanide-doped upconversion nanoparticles coated with human serum albumin (HSA) and a Ru(II) polypyridyl complex for both imaging and PDT purposes. This nanocarrier showed a good cellular uptake as well as an enhanced *in vitro* phototoxicity on HeLa and HepG2 cell lines compared to the Ru(II) complex alone.[71] In an alternative approach, Chakrabortty et al. reported the design and *in vitro* evaluation of an engineered HSA molecule functionalized with mitochondria-targeting groups, solubilizing poly(ethylene glycol) (PEG) chains and Ru(II) polypyridyl complexes. This macromolecule demonstrated an impressive

https://doi.org/10.1021/acs.inorgchem.3c01984
Inorg. Chem. 2023, 62, 15510−15526

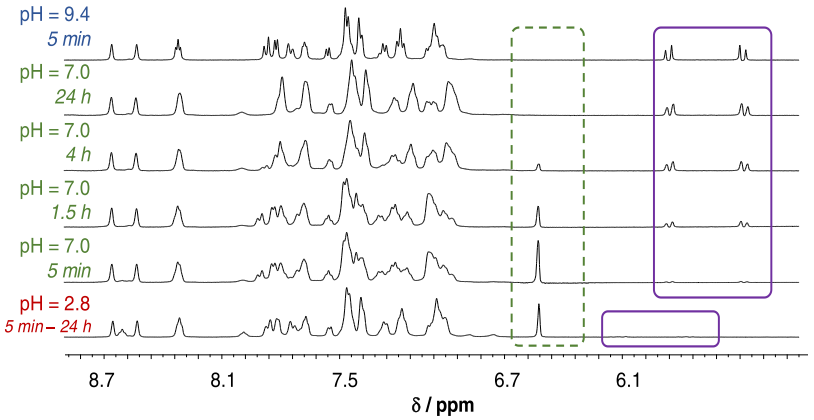

Figure 2. ^{1}H NMR spectra recorded for complex **3** at pH 2.8, 9.4, and 7.0 as a function of time; dashed frame: maleimide C*H*, solid frames: maleamate and at pH 2.8 maleamic acid C*H*. No differences were observed when the complex was incubated for 5 min or 24 h at pH 2.8 {c = 0.5 mM; 10% (v/v) D_2O}.

phototoxic effect in HeLa cells, which was attributed to an enhanced $^{1}O_2$ production yield and a better photostability of the complex associated with favorable mitochondrial localization.[73] Unfortunately, none of these studies investigated the *in vivo* potential of their systems. Moreover, these studies involved the *ex vivo* conjugation of human serum albumin (HSA) to the PS, which requires the use of commercially available HSA. An alternative strategy involves the design of a prodrug incorporating a maleimide (Mal) moiety. Upon intravenous (IV) injection of the prodrug, the Mal group reacts quickly and selectively with the circulating albumin's cysteine-34 (Cys-34) sulfhydryl group, leading to the *in situ* formation of a drug−albumin conjugate. This method therefore allows the development of a simple, well-characterized, low-molecular-weight drug, which is able to benefit from the advantages of albumin-bound drugs.[91,92]

To the best of our knowledge, while this strategy has already been successfully applied to chemotherapeutic complexes of platinum, Ru, and osmium, it has never been applied to vectorize a metal-based PS for PDT applications.[93−100] We believe that Ru(II)-based PSs, and particularly [**Ru(bphen)$_2$dmbipy**][**PF$_6$**]$_2$ or its analogue with chlorides as counterions [**Ru(bphen)$_2$dmbipy**][**Cl**]$_2$ (**1**), could greatly benefit from *in situ* albumin conjugation to improve its tumor accumulation. Therefore, in this article, we describe the synthesis, *in vitro*, and *in vivo* characterization of the first Ru(II) polypyridyl complexes containing a Mal function for *in situ* albumin conjugation. The Mal function was either directly added onto the complex or spaced using a hydrophilic poly(ethylene glycol) (PEG) linker to further improve its aqueous solubility and blood circulation time yielding, respectively, [**Ru(bphen)$_2$dmbipyMal**][**Cl**]$_2$ (**2**) (dmbipyMal = 4-maleimidomethyl-4′-methyl-2,2′-bipyridine) and [**Ru(bphen)$_2$dmbipyPEGMal**][**Cl**]$_2$ (**3**) (PEGMal = *N*-(1-(2,5-dioxo-2,5-dihydro-1*H*-pyrrol-1-yl)-2-oxo-6,9,12,15,18-pentaoxa-3-azaicosan-20-yl)-4-oxopentanamidyl). Of note, we have already described complex **2** in another study, albeit it was used only as an intermediate to the synthesis of a peptide-conjugated PDT PS.[37] We show that all three complexes can bind noncovalently to albumin, and only **2** and **3** exhibit the capability of covalently binding to the protein. The three complexes were then characterized *in vitro* and in a preliminary *in vivo* experiment in tumor-bearing mice to evaluate the potential of this targeting strategy.

RESULTS AND DISCUSSION

The ligand 4-aminomethyl-4′-methyl-2,2′-bipyridine was synthesized as previously reported from 4-bromomethyl-4′-methyl-2,2′-bipyridine with hexamethylenetetramine.[101] The precursor [Ru(bphen)$_2$]Cl$_2$ was prepared by the reduction of Ru(III)Cl$_3$ and substitution with bphen in the presence of LiCl. Following this, the [**Ru(bphen)$_2$dmbipyNH$_2$**][**PF$_6$**]$_2$ complex was obtained by a coordination reaction of the precursor with the above-mentioned ligand. The desired [**Ru(bphen)$_2$dmbipyMal**][**PF$_6$**]$_2$ complex was then obtained using maleic anhydride condensation on the amine (Scheme S1). In parallel, [**Ru(bphen)$_2$dmbipyNH$_2$**][**PF$_6$**]$_2$ was conjugated to a PEG$_5$ linker generated as previously described,[102−105] which was activated as an NHS-ester using standard conditions. The Mal moiety was finally added onto the linker using 2,5-dioxopyrrolidin-1-yl 2-(2,5-dioxo-2,5-dihydro-1*H*-pyrrol-1-yl)acetate (Scheme S1). The compounds were then converted into their chloride salts using a counterion exchange resin to yield complexes **2** and **3**. The identity of the compounds was confirmed by ^{1}H, ^{13}C NMR, and high-resolution mass spectrometry (HRMS) (Figures S1−S10), and the purity was confirmed by elemental analysis. The control complex [**Ru(bphen)$_2$dmbipy**][**PF$_6$**]$_2$ was obtained in a previous study and also converted to the dichloride salt using a counterion exchange resin to give complex **1**. Complexes were used as racemic mixtures of the △ and Λ isomers.

Solubility and Stability. Complexes **1** and **2** showed a good aqueous solubility (≥1 mM), which decreases significantly in buffered media like 15 mM phosphate or phosphate-buffered saline (PBS) at pH 7.40 or even in the presence of 0.1 M KCl. Moderate (*ca.* 7%) precipitation takes place on the basis of the observed decrease in the UV−visible (UV−vis) absorption spectra (see Figure S11A for **2**) even at complex concentrations of 20 μM after 24 h in PBS buffered samples. We have already observed this behavior with analogous complexes in previous studies. We hypothesized that a high anion concentration decreases the repulsive interaction between the positively charged complexes, leading to their aggregation.[37,40] Additionally, as we previously observed, the presence of HSA in buffered media could prevent the precipitation of complexes **1** and **2** for at least 2 days (see UV−vis spectra in Figure S11B).[37,40] In contrast, complex **3**, which includes a hydrophilic PEG spacer, suffers from only a

https://doi.org/10.1021/acs.inorgchem.3c01984
Inorg. Chem. 2023, 62, 15510−15526

Table 1. *n*-Octanol/Aqueous Phase Distribution Coefficients at pH 7.40 (Expressed as log $D_{7.40}$) Determined for **1**−**3**, $[Ru(phen)_3]Cl_2$ (Ru-phen) and $[Ru(bpy)_3]Cl_2$ (Ru-bpy) at 25 °C

aqueous medium	1	2	3	Ru-phen[a]	Ru-bpy[b]
H_2O[c]	−0.03 ± 0.02[d]	+0.81 ± 0.05	+0.82 ± 0.05	−1.6 ± 0.1[e]	<−1.7
0.1 M NaCl[c]	>+3.7	>+3.7	+2.4 ± 0.1		
PBS	>+3.7	>+3.7	+2.3 ± 0.1	−1.30 ± 0.05[f]	<−1.7[g]
15 mM phosphate	+1.5 ± 0.1	+2.3 ± 0.1	+1.1 ± 0.1	−1.5 ± 0.1	<−1.7

[a]log $D_{7.40}$ = −1.09 in 15 mM phosphate and 1 M NaCl. [b]log $D_{7.40}$ < −1.7 in 15 mM phosphate and 1 M NaCl. [c]pH between 6.5 and 8.0. [d]Reported partition coefficient: log *P* = + 0.48 in water.[24] [e]Reported partition coefficient: log *P* = −1.5 in water.[109] [f]Reported partition coefficients: log *P* = −1.1 in PBS,[110] log *P* = −0.33 solvent not reported.[109] [g]Reported partition coefficients: log *P* = −1.21 in PBS,[111] log *P* = −0.41 solvent not reported.[109]

rather moderate decrease in its aqueous solubility in the presence of PBS components. A concentration of 100 μM complex **3** was attainable in this medium. Overall, all studied complexes displayed an acceptable solubility at a concentration of 20 μM in PBS over a 3 h time span (96% of **1** and **2**, and 100% of **3** remained in solution). At the same time, pure aqueous stock solutions of **1** and **2** were proven to be stable for at least 3 days based on the ^{1}H NMR measurements (spectra not shown). However, when the pH was set to 7.4, the hydrolysis of the maleimide group in complex **2** took place, as signals corresponding to a maleamate group formed (Figure S12). Analogously, aqueous stock solutions of **3** were stable in slightly acidic solutions for at least 24 h, according to the ^{1}H NMR spectra depicted in Figure 2. However, at pH 7.4 and 7.0, complex **3** behaved as complex **2** and maleamate formed in a somewhat slower process (Figure 2). A negligible amount of maleamate could be detected at neutral pH for the freshly prepared (5 min) sample, while the hydrolysis progressed to 37, 62, and 100% at time points 1.5, 4, and 24 h, respectively. The hydrolysis appeared even faster at a higher pH of 9.4, which suggests that the hydrolysis rate is pH-dependent, as it was proven for alkyl-maleimides.[106] Noteworthily, the hydrolysis of the present compounds is faster (*ca.* 52%/1 h for **2** and 62%/4 h for **3**) compared to that of ethylmaleimide reported at pH 7.16 and 30 °C ($k_{obs} \approx 10^{-5}$ 1/s, $t_{1/2} \approx 19$ h).[106,107] Therefore, stock solutions of **3** used for *in vitro* experiments were prepared in a slightly acidic solution and used within 12 h. Additionally, stability studies made on complex **2** in Eagle's minimal essential (EMEM) cell culture medium at pH 7.4 showed interaction of **2** with EMEM components within 30 min, and hydrolysis to maleamate was initially suppressed (see Figure S13). These results, however, should be treated with caution because some precipitate also formed in the NMR tube. Overall, complexes **2** and **3** appear to slowly hydrolyze in an aqueous medium under physiologic conditions. However, as we expect the Mal group to react quickly and selectively with the albumin contained both in complete culture medium and in blood, this instability might not dramatically affect the performances of the complexes.

Lipophilicity. The lipophilic or hydrophilic character is an important property influencing the ability of a drug candidate to penetrate biological membranes. The shake-flask method was used for the determination of the *n*-octanol/water partition of the Ru(II) complexes. The complexes $[Ru(phen)_3]Cl_2$ and $[Ru(bpy)_3]Cl_2$ were used as references. Table 1 exhibits the logarithm of the distribution coefficient of the complexes determined at pH 7.40 (log $D_{7.40}$). Interestingly, the lipophilicity of complexes **1**−**3** appears to be highly dependent on the salt content of the aqueous medium as previously observed.[40] **1** shows a slight preference for the aqueous phase over the nonpolar solvent (log *D* = −0.03) when no extra salt is added in the aqueous fraction, while it becomes extremely lipophilic in PBS buffer (log *D* > +3.7). A log *D* = +0.48 was reported by Mazuryk et al. for **1** dissolved in water.[108] Experiments were repeated with the two main components of PBS separately, *i.e.*, with 0.1 M NaCl and 15 mM phosphate. The results showed a more pronounced role of the chloride ions over the phosphate (see Table 1). The same tendency was observed for complexes **2** and **3**. Ion pair formation most probably takes place between the positively charged complexes and anions like Cl^- and $H_2PO_4^-/HPO_4^{2-}$, leading to a reduced aqueous partition. Phenyl substitution of the coordinating 1,10-phenanthrolines at positions 4 and 7 might be responsible for this phenomenon through π-stacking since the lipophilicity of the nonsubstituted complexes $[Ru(phen)_3]Cl_2$ and $[Ru(bpy)_3]Cl_2$ do not display a significant dependency on the electrolyte concentration of the aqueous phase. Both appear to be rather hydrophilic even in the presence of 1 M NaCl and 15 mM phosphate (log $D_{7.40}$ = −1.09 and <− 1.7, respectively).

Since the log *D* of a drug is related to the putative partitioning between lipid membrane and blood plasma, the log *D* values determined in *n*-octanol−PBS buffer system can be considered as more realistic. The results of lipophilicity measurements for complexes **1**−**3** show that they are highly lipophilic, which suggests that their cellular uptake *via* passive transport is possible.

Albumin-Binding Studies. In order to evaluate the ability of the complexes to bind albumin, complexes **1**−**3** were incubated with bovine serum albumin (BSA) in a 2:1 molar excess. BSA was initially used as a model for HSA since it bears the same cysteine at position 34. The mixtures were then dialyzed against distilled water to remove any unbound complex and subjected to matrix-assisted laser desorption ionization time-of-flight (MALDI-TOF) mass spectrometry, using BSA as a control. While BSA can be observed as a single peak in the 60−70 kDa region (mean mass of 66 332 Da), an additional peak could be observed when complexes **2** and **3** were incubated with BSA (Figure S14). This would suggest that the complexes were successfully covalently bound to BSA. However, the same phenomenon was observed for complex **1**. The additional peak observed could therefore represent a noncovalent complex between BSA and the respective compounds, although it is surprising that such a complex would resist the ionization process. We therefore cannot exclude that ion pairing between BSA and free complexes occurred in plasma during ionization. Thus, a more in-depth study was performed by using spectroscopic techniques. Of note, HSA was used in the following experiments to better represent what could happen in human patients.

https://doi.org/10.1021/acs.inorgchem.3c01984
Inorg. Chem. 2023, 62, 15510−15526

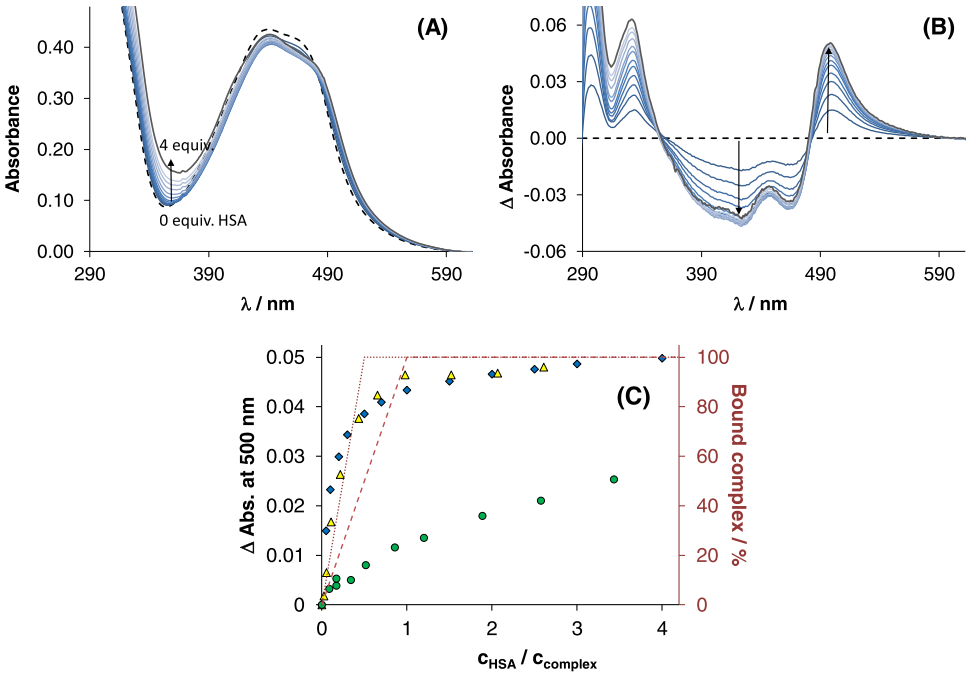

Figure 3. UV−vis absorbance spectra of **1** in the presence of increasing amounts of HSA (A). Derived difference spectra of the same system (B) and absorbance changes of **1** (♦), **2** (△), and **3** (●) at 500 nm plotted together with quantitative binding curves corresponding to one (red dashed line) and two (red dotted line) binding sites on the protein. {$c_{complex}$ = 20 μM; c_{HSA} = 0−80 μM; pH = 7.4 (PBS); 25 °C}. Difference spectra are calculated as follows: $Absorbance_{(complex\text{-}HSA\ mixture)} - Absorbance_{(complex\ alone)} - Absorbance_{(HSA\ alone)}$.

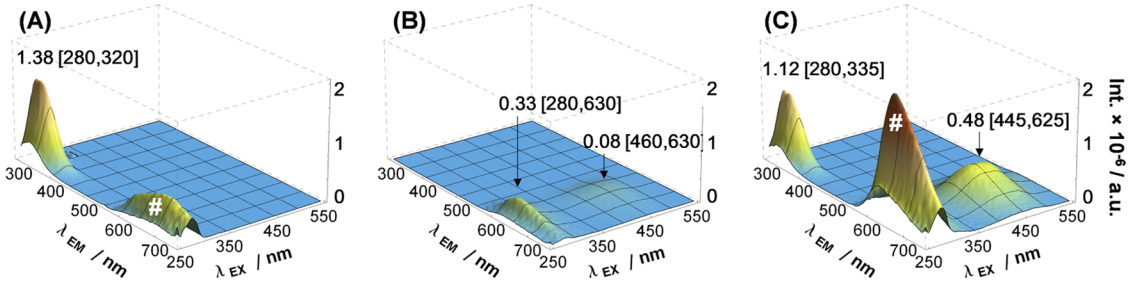

Figure 4. Three-dimensional luminescence spectra of HSA (A), **2** (B), and the HSA−**2** (1:1) (C) system. Peak intensities (int.) and wavelength coordinates ([λ_{EX}, λ_{EM}]) are indicated in the figure; peaks with symbol # originate (partly) from the second-order diffraction effect of the monochromator {c_{HSA} = $c_{complex}$ = 5 μM; pH = 7.40 (PBS); 25 °C; spectra are corrected by self-absorbance and inner filter effect}.

To study the interaction of complexes 1−3 with albumin, we recorded the UV−vis spectra of the complexes in the presence of HSA to follow protein adduct formation processes. Figure 3 shows a minor difference of **1** upon the addition of increasing amounts of HSA in a wavelength range where the protein does not absorb light. The binding process takes place rapidly as the equilibrium is reached within 1−2 min. The spectrum profile of the albumin-bound complex is practically identical to the one recorded in *n*-octanol (see Figure S15A). This observation suggests that the metal complex is accommodated in one or more of the hydrophobic binding pockets of HSA. The calculated difference between the UV−vis spectra (Figure 3B) indicates two isosbestic points at 356 and 482 nm. The changes of the absorbance difference values at 500 nm (Figure 3C) suggest the existence of more than two binding sites on HSA since quantitative binding curves assuming one (dashed line) or two (dotted line) binding sites plotted in the figure are crossed by the collected absorbance values. Complexes **2** and **3** displayed somewhat different behavior (Figures S16 and S17). Although spectral changes are similar to those observed for complex **1**, no isosbestic points were observed. This observation and the slight differences between the octanolic and HSA-bound spectra (Figure S15B for **2**) strongly support an additional binding mode for complexes **2** and **3** *via* the maleimide moiety (*vide infra*). In the case of complex **2**, the biphasic binding character is clearly seen (Figure S16), while **3** shows a lower binding affinity toward HSA since the same amount of HSA affects the absorbance spectrum of **3** much less than **1** and **2** (Figure 3C).

To further study the binding mode between **1**−**3** and albumin, we exploited the intrinsic luminescence of these Ru(II) polypyridyl complexes.[112] As the three-dimensional luminescence spectra in Figure 4 show, complex **2** has two excitation maxima at 280 and 460 nm and emits light between 550 and 750 nm. A *ca.* 6-fold increase of phosphorescence was observed in the presence of 1 equiv of albumin. On the contrary, the emission peak of HSA at λ_{EM} = 320 nm (that originates mainly from the tryptophan at position 214 (Trp-214) situated near site I in subdomain IIA) is significantly reduced, which is a result of the binding of complex **2** at site I. The very same behavior was obtained for **1**, while **3** quenched only slightly the intrinsic fluorescence of HSA (Figure S18).

https://doi.org/10.1021/acs.inorgchem.3c01984
Inorg. Chem. 2023, 62, 15510−15526

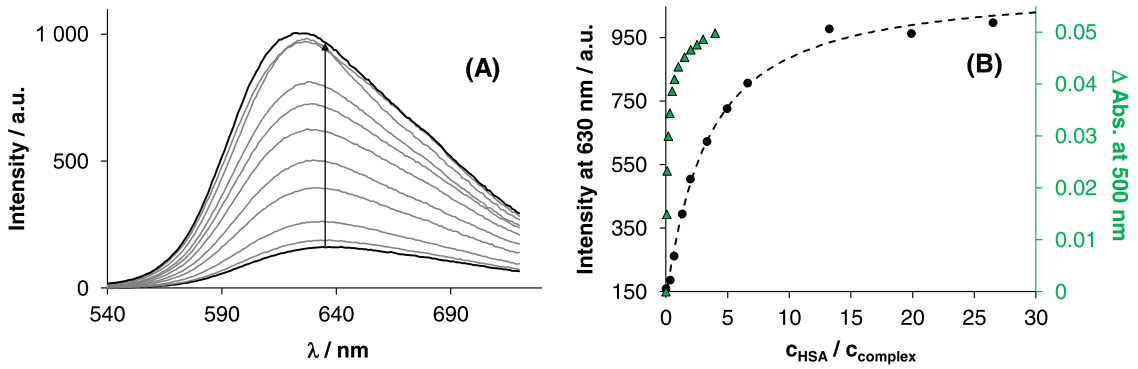

Figure 5. Phosphorescence spectra of **1** in the presence of increasing amounts of HSA (A). Measured and fitted intensities at 630 nm are plotted together with the absorbance changes of **1** titrated by HSA (B) {$c_{complex}$ = 3 μM (fluorometry), 20 μM (UV−vis); λ_{EX} = 445 nm; pH = 7.40 (PBS); 25 °C}.

When the Ru(II) complexes are titrated by HSA, the emission intensity gradually increases, as seen for complex **1** in Figure 5. The emission maximum is gradually shifted toward shorter wavelengths, and the measured intensities reached saturation after the addition of *ca.* 15 equiv of HSA. In Figure 5B, it can be seen that the fluorometric titration curve is far less steep compared to the absorbance-ratio curve; namely, the intrinsic fluorescence of complex **1** is not sensitive to all of the binding events. The titration data could be fitted well with the simple 1:1 binding model; therefore, no more complex binding model was applied. The binding constant of log K' = 5.1 ± 0.1 was calculated with the computer program HypSpec.[100] Complex **2** showed rather similar behavior in the presence of HSA, although a slightly higher binding constant was calculated on the basis of **2**−HSA titrations (Table 2).

Table 2. Conditional Binding Constants (log K') of the Complexes at Binding Sites I and II of HSA and Binding Constant Calculated Based on the Intrinsic Phosphorescence of the Complexes Determined by Spectrofluorometric Measurements {pH = 7.40 (PBS); 25 °C}[c]

log K'[a]	1	2	3
Trp quenching	5.2 ± 0.1[b]	5.2 ± 0.1	
WF displacement	5.5 ± 0.1	5.5 ± 0.1	
DG displacement	5.4 ± 0.1	5.4 ± 0.1	4.5 ± 0.1
intrinsic phosphorescence of the complex	5.1 ± 0.1	5.4 ± 0.1	4.2 ± 0.1

[a]Data presented are the mean value ± standard deviation of at least two independent assays. [b]log K' = 5.09 reported by Mazuryk et al.[24] [c]WF: warfarin and DG: dansylglycine.

Complex **3** behaved again somewhat differently since no shifting of the emission maximum was observed (Figure S19), and a remarkably lower binding constant was calculated (log K' = 4.2 ± 0.1) in comparison to those of **1** and **2**. The measured and calculated data points in Figures 5 and S19 show a strong fit, although it should be noted that the binding of a second (and third) complex on HSA cannot be ruled out. Of note, these results could also be confirmed by following the changes in the lifetime decay of the metal complexes in the presence and absence of HSA (Figure S20). Interestingly, the lifetime of the albumin-bound complexes increased in the absence of molecular oxygen (Table S1). This suggests that the complexes are still able to photosensitize oxygen and thus maintain their photodynamic potential even when bound to albumin.

Binding Location Study. The binding location of the metal complexes in HSA was investigated as the next step. The binding at site I (subdomain IIA) and site II (subdomain IIIA) was studied *via* Trp quenching and site marker displacement experiments. Conditional binding constants computed by HypSpec based on the titration data are listed in Table 2, and fitted quenching curves are depicted in Figure 6.

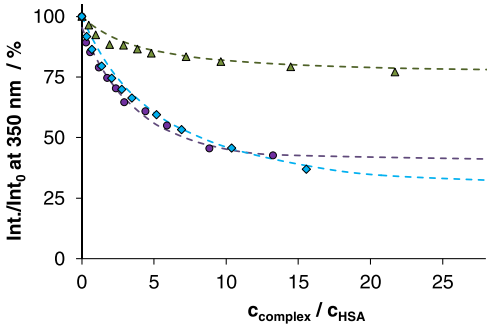

Figure 6. Fluorometric quenching curves recorded for the HSA−**1** (●), HSA-**2** (♦), and HSA−**3** (▲) systems. Dashed lines are the fitted curves calculated on the basis of quenching constants (log K') listed in Table 2 {c_{HSA} = 1 μM; λ_{EX} = 295 nm; pH = 7.40 (PBS); 25 °C}.

Calculated constants for complexes **1** and **2** are fairly similar at both sites. The Trp-214 quenching constant for **1** is in good agreement with the data reported by Mazuryk et al. (log K' = 5.09).[24] The binding site preference and affinity of **3** for HSA were generally different from those of **1** and **2**. Although a Trp-214 quenching constant similar to that of **1** could be calculated for **3** (log K' = 5.4 ± 0.1), the fluorescence of Trp-214 was quenched in only 27% (Figure 6). The warfarin (WF) displacement experiment showed even less alteration in the fluorescence signal of the HSA−WF system upon the addition of **3** (Figure S21). The results of this latter finding and the Trp-214 quenching experiments strongly suggest that the binding of **3** takes place on a place(s) other than site I. The calculated quenching constant (log K' = 5.4 ± 0.1) cannot be handled as a binding constant at site I; therefore, it is not listed in Table 2. Most probably, the allosteric effect of binding of complex **3** can be registered at site I. This phenomenon can also be observed in the reverse experiment; namely, the addition of WF to the **3**−HSA system increases the measured

https://doi.org/10.1021/acs.inorgchem.3c01984
Inorg. Chem. 2023, 62, 15510−15526

emission intensity of the complex (Figure S22). Lifetime measurements (data in Table S1) reveal that this increase originates mainly from the growing lifetime of bound **3**, *i.e.*, the close environment of the bound metal complex changes but not primarily the bound fraction. The other two complexes behaved differently; both **1** and **2** could displace WF from site I, and similar binding constants could be calculated from the displacement data as it was obtained in quenching experiments (Table 2). At the same time, WF addition did not affect the fluorescence of **1**−HSA or **2**−HSA systems (Figure S23).

The binding at site II was investigated in the HSA−dansylglycine (DG)−**complex 1**−**3** ternary systems (see three-dimensional fluorescence spectra and lifetime data collected for HSA−DG−**3** in Figure S24 and Table S2). A relatively low binding constant of **3** at site II could be computed, which is about 1 order of magnitude lower compared to those of **1** and **2** (Table 2). The decrease of HSA-bound **3** fluorescence in the presence of DG seems to originate both from changes of the environment of the bound form (τ_2 decreased from 3060 to 2870 ns) and the slight increase of the bound fraction (α_2: 47% → 53%). In contrast, **1** and **2** could displace DG, but the phosphorescence of these complexes did not change in the reversed type titrations.

To summarize, complexes **1** and **2** can effectively displace WF and DG, apparently occupying sites I and II. On the other hand, **3** can slightly displace DG but not WF. Most probably, its binding at another additional site could be responsible for the elevated phosphorescence of the complex. This particular site seems to be insensitive to any events occurring at sites I or II in the case of complexes **1** and **2**, while the binding site of complex **3** appears to be allosterically connected to sites I and II.

Covalent Binding with Albumin Study. The possible covalent interaction of **2** and **3** with the Cys-34 thiol moiety in albumin was investigated as well. Molecules containing the sulfhydryl group can form a stable thioether conjugate with maleimide at pH between 6.5 and 7.5. HSA, as the most abundant plasma protein having one accessible cysteine (Cys-34), is the most likely target of Mal-linked agents in the blood. *ca.* 20−30% of the Cys-34 thiol groups of HSA are oxidized in the human blood (disulfide bridges are formed with small sulfhydryl compounds);[113] in contrast, commercially available lyophilized HSA is usually oxidized at a higher extent (depending on the recovering and storage conditions). The concentration of the free thiol group of Cys-34 of the protein was determined *via* reaction with 4,4′-dithiodipyridine (DTDP) by spectrophotometry according to our previously reported protocol.[100] Then, 18 ± 2% of Cys-34 of the albumin stock was determined to be present in its nonoxidized form. Since the reaction of the Mal moiety of **2** and **3** with the thiol group of Cys-34 decreases the free thiol content of the protein, the DTDP protocol can be used in order to quantify the sulfhydryl groups of HSA in the presence of the metal complexes (see Figure S25 for UV−vis spectra). Figure 7 shows the changes in free thiol content in HSA as a function of the added equivalents of the complexes. Complex **1** applied as a negative control barely affects the quantity of free thiol groups. On the other hand, the Mal-functionalized complexes **2** and **3** interact to a significant extent with Cys-34. The incubation of **2** with HSA for 3 h (△) or 30 min (▲) did not result in remarkable differences. In addition, the interaction with the native protein did not result in quantitative covalent binding at this site. A similar behavior was observed for **3**.

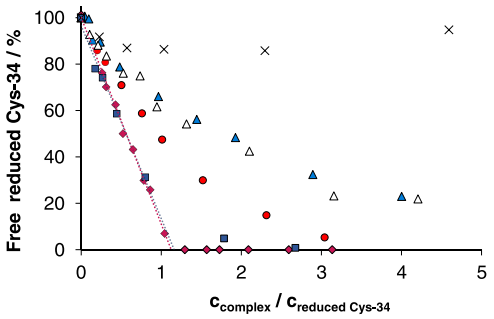

Figure 7. Free Cys-34 SH content of HSA at various **complex**-to-HSA ratios. Symbols denote the following complexes and conditions: open triangle: **2**, 3 h incubation; blue filled triangle: **2**, 30 min incubation; blue filled square: **2**, 0.5% SDS, 30 min; red filled circle: **3**, 30 min; red filled diamond: **3**, 0.5% SDS, 30 min; cross symbol: **1** as a negative control, 30 min {c_{HSA} = 130 μM; $c_{Cys\text{-}34}$ = 23 μM (18% of HSA); pH = 7.00 (100 mM phosphate buffer)}.

Measurements on the sodium dodecyl sulfate (SDS)-denatured protein revealed nearly quantitative interaction of **2** and **3** with the Cys-34 thiol group of HSA. Two scenarios are possible regarding the interaction with the native protein: (i) concurrent binding at other sites in HSA reduces the effective concentration of **2** and **3**, or (ii) the hydrolysis of the Mal moiety competes with the covalent binding of the complexes with Cys-34, which takes relatively longer on the native protein. Complex **3** seems to react more efficiently with the native protein than complex **2**, which could be due to its lower noncovalent binding.

Complexes **2** and **3** were found to react with the Cys-34 thiol group of HSA. Although the interaction is not quantitative, a significant binding *via* the maleimide moiety is highly probable in blood, as well.

Overall, these data suggest that complexes **1** and **2** strongly bind noncovalently to sites I and II of albumin, while this interaction appears significantly weaker for **3**. This could be due to the relatively higher hydrophilicity and steric hindrance provided by the PEG spacer. While both **2** and **3** are able to bind covalently *via* their Mal moiety to the Cys-34 of albumin, the relatively lower noncovalent binding of **3** is counter-balanced with a relatively higher covalent binding efficiency.

Cell Studies. Complex **1** has been described previously as cytotoxic even when cells were incubated in the absence of light exposure, which is an undesired property for a PDT PS.[23,24] We therefore compared the cytotoxic potential of complexes **1**−**3** in the dark on noncancerous immortalized human retinal pigment epithelial cells (RPE-1) following 48 h of incubation. As shown in Table 3, complex **1** induced a significant cytotoxic effect, with an IC_{50} of about 2 μM, which represents the concentration needed to kill 50% of the cells. Of note, the IC_{50} of complex **1** was in the same range as the cytotoxicity measured by Mazuryk et al. on 4T1 cells following 24 h of incubation.[24] In contrast, complexes **2** and **3** were found to be significantly less toxic with IC_{50} values of 74 and 100 μM, respectively. However, following their irradiation at 595 nm, complexes **2** and **3** remained highly phototoxic, with IC_{50} values in the range 4−8 μM on CT26 and RPE-1 cells. Their phototherapeutic index (PI), which represents the ratio between their toxicity in the dark *vs* their toxicity following irradiation, was found to be in the same range as that of complex **1**, if not slightly better. Additional experiments using higher concentrations of the complexes would be required to

https://doi.org/10.1021/acs.inorgchem.3c01984
Inorg. Chem. 2023, 62, 15510−15526

Table 3. IC_{50} Values of Complexes 1−3 under Various Conditions[a]

cell line	compound	A—48 h cytotoxicity (μM)	B—dark (μM)	C—595 nm (μM)	PI
CT26	1	N.D.	5.35 ± 0.08	0.43 ± 0.07	12
	2		>100	8.4 ± 0.6	>12
	3		>100	4.43 ± 0.02	>23
RPE-1	1	2.2 ± 0.1	10.1 ± 0.5	0.8 ± 0.3	13
	2	74 ± 7	>100	4.1 ± 0.1	>24
	3	100 ± 2	>100	4.4 ± 0.2	>23

[a]Column A: cells were incubated continuously with the complexes for 48 h in the dark. Column B: cells were incubated with the complexes for 4 h in the dark, then the medium was exchanged, and cells were incubated for an additional 44 h in the dark. Column C: cells were incubated with the complexes for 4 h in the dark, then the medium was exchanged, cells were irradiated for 2 h at 595 nm (22.47 J/cm^2) and then incubated in the dark for an additional 44 h in the dark. The cell viability was determined using a resazurin assay. Results are presented as means ± standard deviation (SD) of three replicate experiments. PI: phototherapeutic index, N.D.: not determined.

precisely determine their PI. However, while all three complexes appeared to be soluble at the highest concentration tested in culture medium (100 μM), solubility issues will occur at higher concentrations and significantly alter the results. Of note, much higher PIs were previously obtained for Ru(II)-based PSs. For instance, the PI of TLD-1433 was reported to be above 9000 on CT26 cells.[20] However, many other parameters (*e.g.*, tumor accumulation, irradiation wavelength, and light source) are to be taken into account to evaluate the efficiency of a PS.

To rationalize these results, we performed a cellular internalization assay on CT26 cells. Cells were incubated with 5 μM of the complexes **1**−**3** for 4 h. Following a thorough washing procedure, the cells were harvested and digested in nitric acid. Subsequently, the digests were analyzed by inductively coupled plasma mass spectrometry (ICP-MS) to quantify the amount of Ru internalized by the cells. As can be seen in Figure 8, complexes **2** and **3** were significantly less

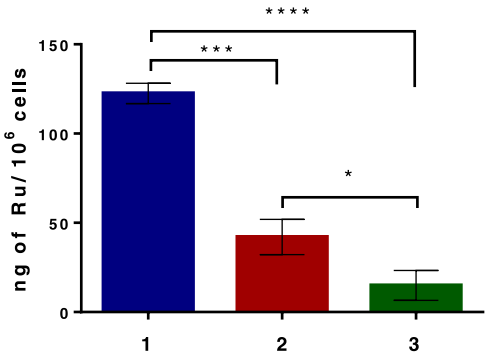

Figure 8. Cellular uptake of complexes **1**−**3** in CT26 cells. The results are presented as mean and SD of three replicates. (*P < 0.05, ***P < 0.0003, ****P < 0.0001, t-test).

internalized than complex **1** (3 and 8 times less, respectively). It is well-known that the lipophilicity of a compound can have a significant effect on its cellular internalization.[114] While this could explain that the more hydrophilic complex **3** is less internalized than complexes **1** and **2**, it does not seem to apply to complex **2**, which is highly hydrophobic. However, as complexes **2** and **3** can covalently bind to albumin, which is present in the culture medium, their reduced internalization could be due to their covalent binding to the bulky protein, which would in turn prevent their uptake *via* passive diffusion. This could be an issue for future *in vivo* applications. If the complexes are not released and subsequently internalized by cancer cells once vectorized to the tumor, they will not be able to reach cellular organelles, such as the nucleus, the mitochondria, or the lysosomes, where they could exert the highest effect.[115]

Nevertheless, the thioether bond in the thiosuccinimide product obtained in the reaction between a thiol and a maleimide can be reversible through thiol-exchange reactions.[116] If the albumin complexes are efficient at accumulating and residing at the tumor site, one could hope that the PS will eventually be released from the protein. On the other hand, this phenomenon could also lead to the premature release of the PS in blood circulation or in sensitive organs, thus increasing off-target toxicity. Such complex processes are however hard to predict using solely *in vitro* experiments, and *in vivo* data could help in understanding the fate of complexes **1**−**3** following their administration.

Animal Studies. We therefore sought to evaluate the biodistribution of complexes **1**−**3** in a CT26 tumor-bearing mouse model. Complexes **1**−**3** were injected into the tail vein at a dose of 2 μmol/kg (corresponding to 2.04, 2.27, and 3.25 mg/kg, respectively). After a given time interval (ranging from 1 min to 24 h), the mice were euthanized and their blood and organs were harvested, digested in nitric acid, and the resulting digests were then analyzed by ICP-MS (3 mice/group). It is important to mention that this method only provides the amount of Ru in tissues but does not give any information about its form (initial complex, degradation product, metabolites, *etc.*). Of note, due to solubility issues, complexes **1** and **2** required the addition of polysorbate 80 (1%) to prevent aggregation, while complex **3** appeared completely soluble at this concentration. The formulation of **1** and **2** with polysorbate was performed using the film rehydration technique, described in more detail in the Experimental Section, while complex **3** was directly solubilized in 5% glucose. While polysorbate might slightly alter the biodistribution of the compounds, we first made sure that it does not prevent the binding of complex **2** with albumin (see Figure S26). As shown in Figure 9A, complexes **1** and **2** were quickly eliminated from the bloodstream within the first 6 h following injection, and only 0.19 and 0.29 μM Ru were detected in the blood 24 h following injection (Figure 9C). In contrast, complex **3** appeared to be eliminated more slowly in the first hours following injection, and 1.61 μM Ru was still detected in the blood at 24 h following injection. The comparable elimination half-lives for the three complexes suggest a similar elimination mechanism. Consequently, the area under the curve (AUC) for complex **3**, which represents the overall exposure of the animals to the complex, is significantly higher than those of complexes **1** and **2**. While we cannot exclude that

https://doi.org/10.1021/acs.inorgchem.3c01984
Inorg. Chem. 2023, 62, 15510−15526

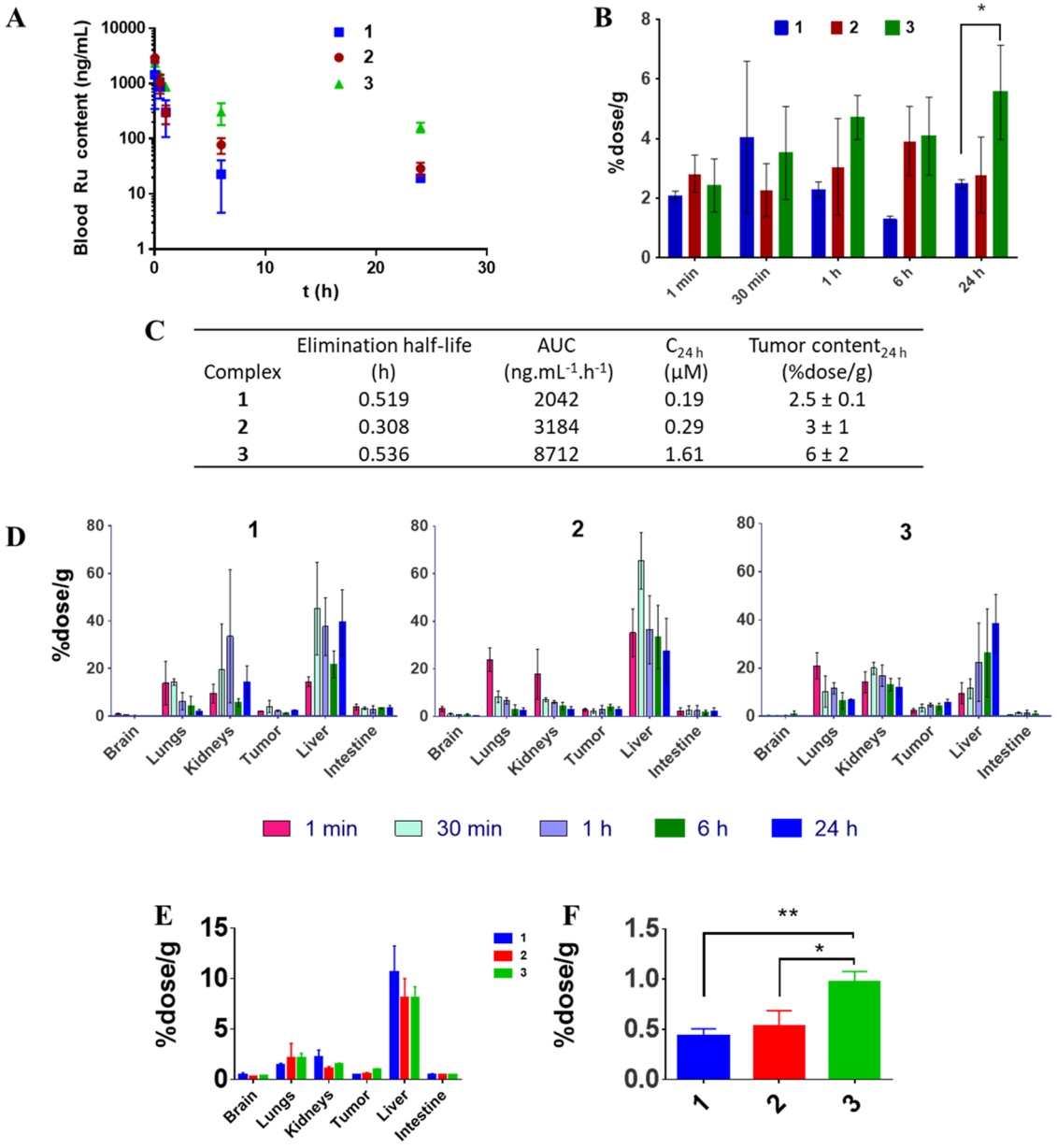

Figure 9. Complexes **1**−**3** were injected IV at a 2 μmol/kg dose of the complexes formulated in 1% polysorbate 80 in PBS (complexes **1** and **2**) or in 5% glucose (complex **3**) (n = 3 mice/time group). In (E) and (F), all three complexes were formulated in 5% glucose. (A) Blood Ru content as a function of time following the administration of complexes **1**−**3** as determined by ICP-MS. (B) Time-dependent Ru tumor content determined by ICP-MS. Data are presented as mean and SD of the % of the total injected dose per gram of tumor (*P < 0.05, t-test). (C) Blood Ru kinetic parameters using a two-phase exponential decay fit. AUC: area under the curve. (D) Time-dependent biodistribution of complexes **1**−**3** in CT26 tumor-bearing mice following the IV injection complexes **1**−**3** (n = 3 mice/time group). Results are presented as the mean and SD of the % of the Ru dose injected per gram of organ. (E) Biodistribution of complexes **1**−**3** in CT26 tumor-bearing mice 48 h following the injection of complexes **1**−**3**. Results are presented as the mean and SD of the % of the total Ru injected dose per gram of the corresponding organ. (F) Ru tumor content determined by ICP-MS 48 h following the injection of complexes **1**−**3**. Data are presented as mean and SD of the % of the total injected dose per gram of tumor (*P < 0.05, **P < 0.005, t-test).

the PEG spacer in complex **3**, or the different formulation used, might be fully responsible for this difference in the blood Ru profiles, its slightly better covalent binding efficiency to albumin (see Figure 7) might also participate in the extension of its blood circulation. Complexes **1**−**3** are distributed in the organs in a similar way and accumulate mainly in the liver and the kidney, suggesting that the elimination of the complexes occurs both by biliary and renal excretion (Figure 9D). All three complexes also appeared to accumulate in the tumors in a comparable manner (Figure 9B). The concentration of complex **3** appeared slightly but significantly higher in the tumor 24 h following injection in comparison to that of complex **1**. Of note, these results are to be taken with caution, considering the small number of animals per group and the high variability of the results.

In order to confirm the trend observed previously, the experiment was repeated on a reduced number of animals to evaluate the biodistribution at a single time point, 48 h following administration of complexes **1**−**3**. As we realized in the meantime that the low solubility of complexes **1** and **2** in

https://doi.org/10.1021/acs.inorgchem.3c01984
Inorg. Chem. 2023, 62, 15510−15526

saline and PBS was not due to their low solubility in water but to the aggregating effect induced by high salt concentrations, we formulated the three complexes in 5% glucose. All three complexes appeared soluble in this vehicle at the concentration required for IV administration (about 400 μM). As shown in Figure 9E,F, complex **3** demonstrated a modestly (*ca.* 2-fold) higher accumulation in the tumor in comparison to complex **1**. Complex **2**, however, did not accumulate significantly more in the tumor in comparison to complex **1**. These results confirm the trend initially observed and show that replacing the polysorbate formulation with 5% glucose did not reverse the superiority of complex **3** over complex **2**.

Overall, these results suggest that adding a Mal moiety to complex **1** had a minor effect on its tumor accumulation. Since this strategy has already been proven as efficient in other metal complexes,[93−95] one could hypothesize that the high hydrophobicity of the three compounds leads to their fast capture in the liver before they had a chance to react with albumin *in vivo*, which gives a slight advantage to the more hydrophilic complex **3**. Given the overall low tumor accumulation and inferior phototoxicity of complexes **2** and **3** in comparison to that of **1**, we decided not to evaluate their PDT efficiency *in vivo*.

CONCLUSIONS

The *in situ* conjugation of drug−maleimide prodrugs to albumin has been described as an efficient strategy to improve the tumor accumulation and the efficiency of antitumor drugs. In this study, we showed that this strategy is not applicable to every compound. *In vitro*, the Ru(II) complexes bearing a Mal moiety described in this work were able to strongly bind noncovalently in several hydrophobic pockets of albumin, as well as covalently to its Cys-34. This property appeared to have a significant and negative impact on their ability to penetrate the cells, which led to a decrease in their phototoxicity. Unfortunately, this decrease was not compensated by a dramatic increase in tumor accumulation *in vivo*, although the addition of a hydrophilic linker slightly improved the blood circulation of the complex. One improvement to this system would be to add a cleavable linker between the maleimide group and the PS, which would enable its release in the tumor microenvironment. Interestingly, the ability of complexes **2** and **3** to react with Cys-34 of albumin appeared to be inversely correlated with their propensity to be bound in the hydrophobic pockets of the protein. This phenomenon may be responsible for a hampered thiol−Mal reaction, which consequently increases the chances for the Mal moiety to be hydrolyzed before it could react with Cys-34. Thus, Mal-prodrugs that strongly bind noncovalently to albumin are to be considered with caution. In addition, incorporating a hydrophilic spacer between the Mal group and the complex appears to be beneficial to both its blood circulation time and its albumin conjugation. Applying the *in situ* Mal-mediated albumin bioconjugation to photosensitizers therefore appears as a promising strategy to improve the efficiency and safety of PDT. Nevertheless, a strong investigation into the interaction between Ru(II) complexes and plasma proteins is needed to design the appropriate system.

EXPERIMENTAL SECTION

Materials. All chemicals were obtained from commercial sources and used without further purification. The Ru(II) complexes *cis*-dichlorotetrakis(dimethyl sulfoxide) Ru(II)[117] and dichlorobis(4,7-diphenyl-1,10-phenanthroline)Ru(II) ($Ru(bphen)_2Cl_2$)[102] and the complexes $[Ru(phen)_3]Cl_2$ and $[Ru(bpy)_3]Cl_2$[118] were synthesized as previously reported. The ligand 5-(aminomethyl)-2,2′-bipyridine was prepared as previously reported.[101] Spectral data were in accordance with the literature. The complex $[\mathbf{Ru(bphen)_2dmbipy}][\mathbf{PF_6}]_2$ was obtained in a previous study[23] and converted to the dichloride salt by elution with MeOH from the ion-exchange resin Amberlite IRA-410 to yield $[\mathbf{Ru(bphen)_2dmbipy}][\mathbf{Cl}]_2$ (**1**). The hydrophilic BOC-protected linker 2,2-dimethyl-4,24-dioxo-3,8,11,14,17,20-hexaoxa-5,23-diazaheptacosan-27-oic acid was prepared as previously described.[102−105] Cells were purchased from the ATCC. Sinapic acid (SA, used as the matrix for MALDI-TOF experiments, was of the highest grade available and used without further purification) was purchased from Sigma-Aldrich Co. Human serum albumin (HSA) containing fatty acids (A8763, essentially globulin-free), KCl, NaCl, NaH_2PO_4, KH_2PO_4, Na_2HPO_4, warfarin (WF), dansylglycine (DG), 2,2′-dithiodipyridine (DTDP), sodium dodecyl sulfate (SDS), and trimethylsilylpropanesulfonate (DSS) were purchased from Sigma-Aldrich. Milli-Q water was used for sample preparation. Samples for albumin-binding studies were prepared in phosphate-buffered saline (PBS) at pH 7.40. Stock solutions of HSA, WF, and DG were prepared as described previously.[119] Pure aqueous stock solutions (c = 1 mM) of the Ru(II) complex were freshly prepared every day, and their concentrations and molar absorptivities were determined based on a weight-in-volume basis. In the HSA binding experiments, these stock solutions were diluted with PBS to get the working solutions (c = 50−200 μM, pH = 7.40). All measurements were carried out at 25.0 ± 0.2 °C.

Instrumentation and Methods. ^{1}H and ^{13}C NMR spectra were recorded on a Bruker 400 MHz NMR spectrometer. Chemical shifts (δ) are reported in parts per million (ppm) referenced to tetramethylsilane (δ 0.00) ppm using the residual proton solvent peaks as internal standards. Coupling constants (J) are reported in hertz (Hz), and the multiplicity is abbreviated as follows: s (singlet), d (doublet), and m (multiplet). Electrospray ionization mass spectrometry (ESI-MS) experiments were carried out using an LTQ-Orbitrap XL from Thermo Scientific (Thermo Fisher Scientific, Courtaboeuf, France) and operated in positive ionization mode, with a spray voltage at 3.6 kV. No Sheath and auxiliary gas were used. The applied voltages were 40 and 100 V for the ion transfer capillary and the tube lens, respectively. The ion transfer capillary was held at 275 °C. Detection was achieved in the Orbitrap with a resolution set to 100,000 (at m/z 400) and a m/z range between 150 and 2000 in profile mode. The spectrum was analyzed using the acquisition software XCalibur 2.1 (Thermo Fisher Scientific, Courtaboeuf, France). The automatic gain control (AGC) allowed accumulation of up to 2×10^5 ions for FTMS scans. Maximum injection time was set to 300 ms, and 1 μscan was acquired. Ten microliters was injected using a Thermo Finnigan Surveyor HPLC system (Thermo Fisher Scientific, Courtaboeuf, France) with a continuous infusion of methanol at 100 μL/min. Elemental microanalyses were performed on a Thermo Flash 2000 elemental analyzer. MALDI-TOF experiments were performed on a MALDI-TOF/TOF UltrafleXtreme mass spectrometer (Bruker Daltonics, Bremen). Mass spectra were obtained in a linear positive ion mode. The laser intensity was set just above the ion generation threshold to obtain peaks with the highest possible signal-to-noise (S/N) ratio without significant peak broadening. All data were processed by using the FlexAnalysis software package (Bruker Daltonics). Fluorescence and phosphorescence lifetime measurements were carried out on a Fluoromax (Horiba Jobin Yvon) spectrofluorometer equipped with a DeltaHub time-correlated single photon counting (TCSPC) system using nanoLED light sources N-295, N-350, and N-460 (Horiba Jobin Yvon). ICP-MS studies were performed using an Element II HR-ICP-MS instrument (Thermo Fisher Scientific).

Synthesis. ***[Ru(bphen)$_2$dmbipyNH$_2$][PF$_6$]$_2$.*** $Ru(bphen)_2Cl_2$ (200 mg, 0.24 mmol, 1.0 equiv) and 5-(aminomethyl)-2,2′-bipyridine (57 mg, 0.29 mmol, 1.2 equiv) were dissolved in a 1:3 mixture of H_2O/ethanol (50 mL) and refluxed overnight under a N_2 atmosphere. The solvent was evaporated, and the residue was dissolved in 10 mL of

https://doi.org/10.1021/acs.inorgchem.3c01984
Inorg. Chem. 2023, 62, 15510−15526

H_2O. A saturated aq. NH_4PF_6 solution was added, and the resulting precipitate was collected by vacuum filtration. The solid was washed with H_2O (50 mL) and Et_2O (50 mL). The product was dried in a high vacuum. Yield: 89%. ^{1}H NMR (400 MHz, CD_3CN) δ = 8.59 (s, 1H), 8.44 (s, 1H), 8.29 (d, J = 5.5 Hz, 1H), 8.26 (d, J = 5.5 Hz, 1H), 8.15−8.07 (m, 6H), 7.93 (d, J = 5.9 Hz, 1H), 7.74−7.70 (m, 3H), 7.62−7.47 (m, 22H), 7.39 (dd, J = 5.9, 1.7 Hz, 1H), 7.24 (d, J = 5.7 Hz, 1H), 4.38 (s, 2H), 2.53 (s, 3H); ^{13}C NMR (100 MHz, CD_3CN) δ = 158.4, 156.6, 152.9, 152.6, 152.4, 152.3, 151.8, 151.3, 149.5, 149.4, 149.4, 148.9, 148.7, 148.6, 142.9, 136.2, 136.2, 130.3, 130.2, 130.0, 130.0, 129.6, 129.5, 129.4, 129.4, 129.3, 127.4, 126.8, 126.7, 126.6, 126.4, 125.6, 124.5, 42.8, 20.8.

[Ru(bphen)$_2$dmbipyMal][Cl]$_2$ (2). [**Ru(bphen)$_2$dmbipyMal**]-[**PF$_6$**]$_2$ was synthesized as previously described. ^{1}H and ^{13}C NMR spectra were in accordance with the reported data.[37]

The counterion PF_6^- was exchanged to Cl^- by elution with MeOH from the ion-exchange resin Amberlite IRA-410. Elemental analysis calcd for $C_{64}H_{45}Cl_2N_7O_2Ru + H_2O$ (%): C 67.78, H 4.18, N 8.65; found: C 67.73, H 3.94, N 8.36.

[Ru(bphen)$_2$dmbipyPEGNH$_2$][PF$_6$]$_2$. To a solution of 2,2-dimethyl-4,24-dioxo-3,8,11,14,17,20-hexaoxa-5,23-diazaheptacosan-27-oic acid (0.150 g, 0.31 mmol, 1.00 equiv) in anhydrous dichloromethane (DCM) (5 mL) were added *N*-hydroxysuccinimide (0.043 g, 0.37 mmol, 1.2 equiv) and dicyclohexylcarbodiimide (0.076 g, 0.37 mmol, 1.2 equiv). The mixture was agitated for 15 h at room temperature. The solid was filtered off, and the filtrate was evaporated to yield a transparent oil (0.185 g). To a solution of this oil in anhydrous DCM (2 mL) was added a solution of [**Ru(bphen)$_2$dmbipyNH$_2$**][**PF$_6$**]$_2$ (0.197 mg, 0.16 mmol, 1.00 equiv) and *N*,*N*-diisopropylethylamine (DIPEA) (0.08 mL, 0.48 mmol, 3.0 equiv) in DCM (3 mL). The mixture was agitated in the dark at room temperature under nitrogen for 15 h. The solvent was evaporated, and the residue was dissolved in methanol (10 mL). A saturated solution of NH_4PF_6 was added, and the orange solid was isolated by filtration, washed with cold water and diethyl ether (Et_2O), and finally dried under vacuum. Under nitrogen, the solid was dissolved in DCM (1 mL), and trifluoroacetic acid (0.1 mL) was added. The mixture was agitated at room temperature for 15 h. The solvent was evaporated to dryness, the residue was dissolved in a small amount of methanol, and a saturated solution of NH_4PF_6 was added. The orange solid was isolated by filtration and washed with cold water and Et_2O. The crude product was purified by column chromatography on silica gel with a CH_3CN/aq. KNO_3 (0.4 M) solution (10:1). The fractions containing the product were united, and the solvent was removed. The residue was dissolved in CH_3CN, and undissolved KNO_3 was removed by filtration. The solvent was evaporated, and the product was dissolved in H_2O (20 mL). Upon the addition of NH_4PF_6, the product precipitated as a PF_6 salt. The solid was obtained by filtration and was washed with H_2O (50 mL) and Et_2O (50 mL) to yield [**Ru(bphen)$_2$dmbipyPEGNH$_2$**][**PF$_6$**]$_2$ as an orange powder (85 mg, 0.05 mmol, 58%). ^{1}H NMR (400 MHz, CD_3CN) δ = 8.64 (d, J = 1.7 Hz, 1H), 8.48 (d, J = 1.8 Hz, 1H), 8.28 (t, J = 5.5 Hz, 2H), 8.24−8.15 (m, 4H), 8.11 (t, J = 5.7 Hz, 2H), 7.76 (dd, J = 5.5, 1.4 Hz, 2H), 7.74 (d, J = 6.0 Hz, 1H), 7.71−7.53 (m, 21H), 7.26−7.21 (m, 2H), 7.17 (t, J = 6.1 Hz, 1H), 6.83 (s, 2H), 6.69 (t, J = 5.9 Hz, 1H), 4.56 (d, J = 6.1 Hz, 2H), 3.68−3.61 (m, 2H), 3.59−3.39 (m, 18H), 3.35−3.26 (m, 2H), 3.01 (dd, J = 6.1, 4.3 Hz, 2H), 2.61−2.54 (m, 4H), 2.51−2.46 (m, 2H); ^{13}C NMR (100 MHz, CD_3CN) δ = 174.0, 158.2, 157.6, 153.2, 153.1, 152.9, 152.6, 152.5, 152.2, 151.6, 149.94, 149.87, 149.85, 149.5, 149.31, 149.30, 136.71, 136.68, 136.6, 130.8, 130.72, 130.66, 130.62, 130.57, 130.11, 130.06, 129.9, 129.3, 127.09, 127.05, 127.0, 126.3, 126.2, 122.7, 70.84, 70.82, 70.80, 70.6, 70.5, 70.3, 70.2, 70.0, 67.3, 42.4, 40.6, 39.6, 31.3, 21.3.

[Ru(bphen)$_2$dmbipyPEGMal][Cl]$_2$ (3). Under nitrogen, 2,5-dioxopyrrolidin-1-yl 2-(2,5-dioxo-2,5-dihydro-1*H*-pyrrol-1-yl)acetate (23 mg, 0.09 mmol, 2.0 equiv) was added to a solution of [**Ru(bphen)$_2$dmbipyPEGNH$_2$**][**PF$_6$**]$_2$ (73 mg, 0.045 mmol, 1.0 equiv) and DIPEA (80 mg, 0.068 mmol, 1,5 equiv) in DCM (5 mL). The mixture was agitated at room temperature in the dark for 15 h. The solvent was removed, the residue was dissolved in a small amount of methanol, and a saturated solution of NH_4PF_6 was added. The orange solid was isolated by filtration and washed with cold water and Et_2O. The counterion PF_6^- was exchanged to Cl^- by elution with MeOH from the ion-exchange resin Amberlite IRA-4101 to yield [**Ru(bphen)$_2$dmbipyPEGMal**][**PF$_6$**]$_2$ (**3**) as an orange powder (61 mg, 0.040 mmol, 89%). ^{1}H NMR (400 MHz, CD_3CN) δ = 8.79 (s, 1H), 8.53 (s, 1H), 8.30 (dd, J = 5.5, 2.8 Hz, 2H), 8.23−8.14 (m, 4H), 8.10 (dd, J = 5.5, 3.6 Hz, 2H), 7.76 (dd, J = 5.5, 3.8 Hz, 2H), 7.73 (d, J = 5.9 Hz, 1H), 7.70−7.52 (m, 23H), 7.28−7.17 (m, 3H), 6.78 (s, 2H), 6.68−6.60 (m, 1H), 6.00 (s, 1H), 4.58 (dd, J = 17.6, 6.1 Hz, 1H), 4.51 (dd, J = 17.6, 6.1 Hz, 1H), 4.03 (s, 2H), 3.53−3.34 (m, 20H), 3.31−3.19 (m, 4H), 2.58 (s, 3H), 2.52 (s, 4H). ^{13}C NMR (100 MHz, CD_3OD) δ = The counterion PF_6^- was exchanged to Cl^- by elution with MeOH from the ion-exchange resin Amberlite IRA-4101. ^{13}C NMR (100 MHz, CD_3CN) δ = 175.6, 174.6, 171.9, 169.2, 158.8, 158.3, 153.3, 153.0, 152.5, 152.2, 150.74, 150.68, 149.9, 149.8, 137.1, 137.0, 135.7, 131.1, 131.02, 130.94, 130.88, 130.4, 130.3, 130.0, 127.7, 127.4, 127.0, 126.8, 71.5, 71.3, 71.2, 70.4, 70.3, 58.3, 43.0, 40.64, 40.55, 40.4, 31.7, 31.4, 21.4, 18.4. ESI-HRMS (pos. detection mode): calcd for $C_{82}H_{78}N_{10}O_{10}Ru$ m/z $[M]^{2+}$ 732.2467; found: 732.2481. Elemental analysis calcd for $C_{64}H_{45}Cl_2N_7O_2Ru + 5H_2O$ (%): C 60.59, H 5.46, N 8.62; found: C 60.68, H 5.46, N 8.75.

Physicochemical Properties. *^{1}H NMR Spectroscopy for Stability Studies.* ^{1}H NMR spectroscopic studies were carried out on a Bruker Avance III HD Ascend 500 Plus instrument. Complexes were dissolved in 0.5 mM concentration in water, PBS buffer, 5 mM phosphate (pH 7.4), or EMEM, and 10% (v/v) D_2O was added to the samples. Spectra were recorded with the WATERGATE water suppression pulse scheme using DSS as an internal standard.

Lipophilicity and Membrane Permeability. Distribution constants (D) of **1**, **2**, and **3** were determined by the traditional shake-flask method in *n*-octanol/buffered aqueous solution at pH 7.40 (PBS, or 15 mM phosphate buffer) and in water containing 0 or 0.1 M KCl as described previously.[90,120] The complexes were dissolved in *n*-octanol presaturated aqueous solution at *ca.* 20 μM concentrations. Aqueous phases and water-presaturated *n*-octanolic phases were gently mixed in 1:1 or 100:1 volume ratios with a Heidolph Reax 2 overhead shaker (∼20 rpm) for 2 h. After separation, UV−vis spectra of the compounds in the aqueous phase were compared to those of the original aqueous solution, and D values of the compounds were calculated according to the following equation

$$D = \left[\frac{\mathrm{Abs}_{(\text{stock. sol.})}}{\mathrm{Abs}_{(\text{aqueous phase after separation})}} - 1\right] \times \frac{V_{(\text{aqueous phase})}}{V_{n\text{-octanol phase}}} \quad (1)$$

An Agilent Cary 8454 diode array spectrophotometer was used to measure the UV−vis spectra in the interval 200−800 nm.

Albumin Interaction. *MALDI Sample Preparation.* Complexes **1**−**3** from stock solutions in ethanol were added to a 100 μM solution of BSA in PBS at a final complex concentration of 200 μM (final ethanol concentration: 5%). The mixtures were agitated at 450 rpm, 37 °C for 2 h in a Thermomixer (Eppendorf). The mixtures were then dialyzed against 2 L distilled water for 24 h (3 buffer exchanges) using dialysis cassettes (Slide-A-Lyzer MWCO 10 kDa, Thermo Fisher).

The matrix solution was prepared at a concentration of 45 mM in H_2O/CH_3CN/trifluoroacetic acid 1/1/0.1.

The samples were prepared by mixing the BSA-complex mixture solution with a matrix solution at a volume ratio of 1:9.

UV−Visible Spectrophotometric and Circular Dichroism Spectroscopic Measurements. UV−visible (UV−vis) spectrophotometry was utilized to follow the stability of the complexes in various aqueous solutions and monitor their interaction with HSA on an Agilent Cary 8454 diode array spectrophotometer and an Agilent Cary 3500 spectrophotometer in the wavelength range between 200 and 800 nm. Samples contained *ca.* 20 μM metal complex dissolved in various buffer systems (PBS, phosphate) or in water. In protein binding studies, a constant amount of complex was titrated by HSA (0−80 μM).

The interaction of the metal complexes at the Cys-34 residue of HSA was investigated *via* the DTDP method described in our former

https://doi.org/10.1021/acs.inorgchem.3c01984
Inorg. Chem. 2023, 62, 15510−15526

work.[100] The available cytosine thiol content in HSA was determined to be 18%. Complex binding was tested in the following setup: 130 μM HSA (23 μM free thiol) and various amounts of complex (0−120 μM) were incubated for 3 h or 30 min at pH 7.00 (100 mM phosphate), and the UV−vis spectra were recorded (a), then 110 μM DTDP was added, and the UV−vis spectra were measured again after another 40 min waiting time (b). The spectrum of the colored reaction product 2-thiopyridone (2-TP) was derived by the subtraction of the spectrum (a) from the spectrum (b). A blank experiment with **1** was carried out in addition to a control experiment. The effect of protein unfolding on the thiol binding of **2** and **3** was studied by the addition of 0.5% (w/w) SDS to the protein prior to its reaction with the complex.

Spectrofluorometric Measurements. Samples were measured in 1 × 1 cm^2 cells. PBS buffer was used for sample preparation, and emission spectra were recorded after 5 min incubation. Four kinds of experiments were carried out: (i) 1 μM HSA and various amounts of complex (from 0 to 20 equiv) were used for quenching experiments; and (ii) fluorescence of site markers WF and DG was measured in samples containing 1 μM HSA, 1 μM marker, and 0−20 μM compound; intrinsic fluorescence of the complexes was followed as well by applying (iii) 5 μM complex and various HSA concentrations (0−110 μM) or (iv) 5 μM complex, 5 μM HSA, and various site markers (WF and DG) concentrations (0−160 μM). Instrumental parameters are listed in Table S3. The computer program HypSpec[121] was utilized for the calculation of formation constants for HSA−compound adducts, as described in our former work.[119,122] Corrections for self-absorbance and inner filter effect were done as described in our former work using the formula suggested by Lakowicz.[112]

Time-Resolved Fluorescence Measurements. Ludox (from Sigma-Aldrich) was used as a scatter to obtain the instrument response function. The background (obtained with blank samples) was subtracted from the decay. The program DAS6 (version 6.6; Horiba, Jobin Yvon) was used for the analysis of the experimental fluorescence decays. The fluorescence intensity decay over time is described by a sum of exponentials as the following equation shows

$$I(t) = \sum_{i=1}^{n} \alpha_i \exp\left(\frac{-t}{\tau_i}\right) \quad (2)$$

where α_i and τ_i are the normalized amplitude and lifetime of component i, respectively. From these parameters, the fraction of emitted light by each component i can be calculated through the equation

$$f_i = \frac{\alpha_i \tau_i}{\sum (\alpha_i \tau_i)} \quad (3)$$

The goodness of the fit was judged from a χ_R^2 value close to 1.0 and a random distribution of weighted residuals. See details on the instrument settings for different kinds of fluorophores in Table S3.

***In Cellulo* Experiments.** *Cell Culture.* CT26 cells were cultured in DMEM medium (Gibco, Life Technologies) supplemented with 10% of fetal calf serum (Gibco) and 100 U/mL penicillin−streptomycin mixture (Gibco) and maintained in a humidified atmosphere at 37 °C and 5% CO_2. RPE-1 cells were cultured in DMEM−F12 medium (Gibco, Life Technologies) supplemented with 10% of fetal calf serum (Gibco) and 100 U/mL penicillin−streptomycin mixture (Gibco) and maintained in a humidified atmosphere at 37 °C and 5% CO_2.

Forty-Eight-Hour Cytotoxicity Assay. Cells were seeded in triplicate plates in 96-well plates at a 4000 cells/well density in 100 μL and were incubated at 37 °C in 5% CO_2 for 24 h. The medium was replaced with increasing concentrations of test compounds in 100 μL of fresh medium, and cells were incubated at 37 °C in 5% CO_2 for 48 h. The medium was replaced with 100 μL of fresh medium containing 0.2 mg/mL of resazurin. After 4 h of incubation at 37 °C in 5% CO_2, the fluorescence intensity of resorufin was read at 590 nm with an excitation wavelength of 540 nm using a SpectraMaxM5 microplate reader (Molecular Devices). Data were fitted using GraphPad Prism V6.07 Software. Fluorescence intensities (Y values) were plotted against compound concentrations (X values). X values were transformed into log(X) values. Y values were normalized by setting 100% cell viability for the highest fluorescence intensity and 0% cell viability for the lowest fluorescence intensity in each data set. IC_{50} was calculated by nonlinear regression using the algorithm "log(inhibitor) *vs* normalized response".

Phototoxicity Assay. Cells were seeded in triplicate plates in 96-well plates at a 4000 cells/well density in 100 μL and were incubated at 37 °C in 5% CO_2 for 24 h. The medium was replaced with increasing concentrations of test compounds in 100 μL of fresh medium, and cells were incubated at 37 °C in 5% CO_2 for 4 h. The medium was then replaced with fresh medium, and wells were individually irradiated at 595 nm for 2 h (22.47 J/cm^2) using a LUMOS-BIO photoreactor (Atlas Photonics). Control plates were kept in the dark in a non-CO_2 incubator for 4 h. Cells were then incubated for an additional 44 h at 37 °C in 5% CO_2. The medium was replaced with 100 μL of fresh medium containing 0.2 mg/mL of resazurin. After 4 h of incubation at 37 °C in 5% CO_2, the fluorescence intensity of resorufin was read at 590 nm with an excitation wavelength of 540 nm using a SpectraMaxM5 microplate reader (Molecular Devices). Data were fitted using GraphPad Prism V6.07 Software. Fluorescence intensities (Y values) were plotted against compound concentrations (X values). X values were transformed into log(X) values. Y values were normalized by setting 100% cell viability for the highest fluorescence intensity and 0% cell viability for the lowest fluorescence intensity in each data set. IC_{50} was calculated by nonlinear regression using the algorithm "log(inhibitor) *vs* normalized response".

Cellular Uptake. A total of 5 × 10^6 CT26 cells (5 × 10^6) were seeded in 10 cm Petri dishes (10 mL/dish) and were incubated at 37 °C in 5% CO_2. The next day, the medium was replaced with 5 μM complex dilution in 10 mL of culture medium, and the dishes were incubated for 4 h at 37 °C in 5% CO_2. Cells were washed three times with cold PBS, trypsinized, and harvested, and a 10 μL aliquot of each cell suspension was sampled for accurate counting. The cell suspensions were centrifuged, and the supernatant was discarded. The pellets were digested in 100 μL of 70% HNO_3 at 65 °C for 24 h and then diluted in 5 mL of Milli-Q water (final HNO_3 concentration: 1.4%). The Ru content in each sample was determined by ICP-MS. The amount of Ru detected in the digests was transformed from ppb into ng and normalized using the total number of cells digested. Experiments were performed in triplicate.

***In vivo* Studies.** *Animals.* This study was carried out in accordance with the EU regulations and approved by the Ethical Commission of the faculty of Pharmaceutical and Biological Sciences Paris-Descartes (agreement number: E-75-06-02).

Eight-week-old Balb/c mice were provided by Janvier Lab and housed with food and water supplied *ad libitum* in a 12-h day/night cycle.

Formulation in Polysorbate 80. A total of 1.74 μmol of the test compound and 50 mg of polysorbate 80 were dissolved in 5 mL of anhydrous ethanol. The solution was concentrated to dryness under a vacuum in a round-bottom flask to yield an orange viscous film that was further dried at 40 °C under a vacuum for 10 min. The film was then rehydrated in 5 mL of PBS (Gibco). The orange solution was finally sterile-filtered on a 0.2 μm cellulose-acetate membrane (Corning). Test compound concentration was determined by measuring the absorbance of the solution after dilution in acetonitrile at 450 nm in quartz cuvettes using a SpectraMaxM5 (Molecular Devices) spectrophotometer.

[Ru(bphen)$_2$dmbipyMal]Cl$_2$ Conjugation to Albumin Kinetics. A solution of complex **2** (0.2 mg/mL) formulated in either 5% ethanol in PBS (Gibco) or 1% polysorbate 80 in PBS (Gibco) was added to a solution of bovine serum albumin (BSA) (120 mg/mL) in PBS (Gibco). The mixture was shaken at 450 rpm at 37 °C in a Thermomixer (Eppendorf). At each time point, 300 μL of the mixture was added to 800 μL of CH_3CN. The mixture was vortexed for 5 s and then centrifugated for 5 min at 10,000*g*. The absorbance of the supernatants was recorded at 450 nm in a quartz cuvette using a

https://doi.org/10.1021/acs.inorgchem.3c01984
Inorg. Chem. 2023, 62, 15510−15526

SpectraMaxM5 (Molecular Devices) spectrophotometer. The experiment was performed in triplicates. %conversion was calculated using the following formula

$$\% \text{ conversion} = \frac{\text{Abs}_{t0} - \text{Abs}_{t}}{\text{Abs}_{t0}}$$

Biodistribution Study. Fifteen 10-week-old BALB/c mice were implanted subcutaneously in both flanks with two CT26 tumor fragments with a diameter of 1 mm, previously extracted from donor mice.

After 8 days, mice were randomly divided into five groups and injected intravenously in the caudal vein with 2 μmol/kg of test compound formulated in 1% polysorbate 80 in PBS (complexes **1** and **2**) or 5% glucose in water (complex **3**). After 1 min, 30 min, 1 h, 6 h, and 24 h, mice were sacrificed, and relevant organs, including blood, tumors, liver, kidneys, intestine, lungs, and brain, were harvested and weighed. Organs were then digested in 70% nitric acid at 65 °C for 24 h. Digests were diluted 100 times in 1% HCl, and Ru contents were determined by ICP-MS. The amount of Ru detected in organ digests was transformed from ppb into ng of Ru and expressed as a % of the injected dose/g of organs. Tumor Ru contents are presented as an average of left and right tumors Ru content. Kinetic parameters were calculated using GraphPad Prism V6.07 Software by fitting the blood Ru content as a function of time, using a two-phase exponential decay equation. The 48 h biodistribution experiment was performed similarly, but complexes **1**−**3** were all formulated in 5% glucose in water for comparison purposes. Three mice were used for each compound.

■ ASSOCIATED CONTENT

Supporting Information

The Supporting Information is available free of charge at https://pubs.acs.org/doi/10.1021/acs.inorgchem.3c01984.

Synthesis scheme (Scheme S1); ^{1}H, ^{13}C NMR spectra, and HRMS (Figures S1−S10); complex-albumin additional figures (Figures S11−S22); binding kinetic of complex **2** formulated in polysorbate 80 or ethanol (Figure S23); tables containing fluorescence lifetime parameters (Tables S1−S3) (PDF)

■ AUTHOR INFORMATION

Corresponding Authors

Robin Vinck − *Chimie ParisTech, PSL University, CNRS, Institute of Chemistry for Life and Health Sciences, F-75005 Paris, France*; Phone: +33 1 85 78 41 51; Email: robin.vinck13@gmail.com; www.gassergroup.com

Gilles Gasser − *Chimie ParisTech, PSL University, CNRS, Institute of Chemistry for Life and Health Sciences, F-75005 Paris, France*; orcid.org/0000-0002-4244-5097; Phone: +33 1 85 78 41 51; Email: gilles.gasser@chimeparistech.psl.eu; www.gassergroup.com

Authors

Orsolya Dömötör − *MTA-SZTE Lendület Functional Metal Complexes Research Group, Department of Molecular and Analytical Chemistry, University of Szeged, H-6720 Szeged, Hungary*

Johannes Karges − *Chimie ParisTech, PSL University, CNRS, Institute of Chemistry for Life and Health Sciences, F-75005 Paris, France*; orcid.org/0000-0001-5258-0260

Marta Jakubaszek − *Chimie ParisTech, PSL University, CNRS, Institute of Chemistry for Life and Health Sciences, F-75005 Paris, France*

Johanne Seguin − *Université Paris Cité, UTCBS, INSERM, CNRS, 75006 Paris, France*; orcid.org/0000-0001-5689-7046

Mickaël Tharaud − *Biogéochimie à l'Anthropocène des Eléments et Contaminants Emergents, Institut de Physique du Globe de Paris, 75005 Paris, France*; orcid.org/0000-0001-6131-655X

Vincent Guérineau − *Institut de Chimie des Substances Naturelles, CNRS UPR2301, Université Paris-Sud, Université Paris-Saclay, 91198 Gif-sur-Yvette, France*

Kevin Cariou − *Chimie ParisTech, PSL University, CNRS, Institute of Chemistry for Life and Health Sciences, F-75005 Paris, France*

Nathalie Mignet − *Université Paris Cité, UTCBS, INSERM, CNRS, 75006 Paris, France*

Éva A. Enyedy − *MTA-SZTE Lendület Functional Metal Complexes Research Group, Department of Molecular and Analytical Chemistry, University of Szeged, H-6720 Szeged, Hungary*; orcid.org/0000-0002-8058-8128

Complete contact information is available at: https://pubs.acs.org/10.1021/acs.inorgchem.3c01984

Author Contributions

#R.V. and O.D. contributed equally to this work.

Notes

The authors declare no competing financial interest.

■ ACKNOWLEDGMENTS

This work was financially supported by an ERC Consolidator Grant Photo-MedMet to G.G. (GA 681679) and has received support under the program "'Investissements d"Avenir" launched by the French Government and implemented by the ANR with the reference ANR-10-IDEX-0001-02 PSL (G.G.) and from a Qlife prématuration funding (G.G. and R.V.). Part of the ICP-MS measurements was supported by the IPGP multidisciplinary program PARI and by Paris—IdF region SESAME Grant no. 12015908. The support of the "Lendület" Program (ELKH (Hungary), LP2019-6/2019) is also acknowledged (E.A.E.). O.D. gratefully acknowledges the financial support from a J. Bolyai Research Fellowship (bo-125-20) and the ÚNKP-22-5-SZTE-547—New National Excellence Program.

■ REFERENCES

(1) Dolmans, D. E. J. G. J.; Fukumura, D.; Jain, R. K. Photodynamic Therapy for Cancer. *Nat. Rev. Cancer* **2003**, *3* (5), 380−387.
(2) Bonnet, S. Why Develop Photoactivated Chemotherapy? *Dalton Trans.* **2018**, *47* (31), 10330−10343.
(3) Dougherty, T. J.; Gomer, C. J.; Henderson, B. W.; Jori, G.; Kessel, D.; Korbelik, M.; Moan, J.; Peng, Q. Photodynamic Therapy. *JNCI, J. Natl. Cancer Inst.* **1998**, *90* (12), 889−905.
(4) Henderson, B. W.; Dougherty, T. J. How Does Photodynamic Therapy Work? *Photochem. Photobiol.* **1992**, *55* (1), 145−157.
(5) Plaetzer, K.; Krammer, B.; Berlanda, J.; Berr, F.; Kiesslich, T. Photophysics and Photochemistry of Photodynamic Therapy: Fundamental Aspects. *Lasers Med. Sci.* **2009**, *24* (2), 259−268.
(6) Bonnett, R. Photosensitizers of the Porphyrin and Phthalocyanine Series for Photodynamic Therapy. *Chem. Soc. Rev.* **1995**, *24* (1), 19−33.
(7) O'Connor, A. E.; Gallagher, W. M.; Byrne, A. T. Porphyrin and Nonporphyrin Photosensitizers in Oncology: Preclinical and Clinical Advances in Photodynamic Therapy. *Photochem. Photobiol.* **2009**, *85* (5), 1053−1074.

(8) Heinemann, F.; Karges, J.; Gasser, G. Critical Overview of the Use of Ru(II) Polypyridyl Complexes as Photosensitizers in One-Photon and Two-Photon Photodynamic Therapy. *Acc. Chem. Res.* **2017**, *50* (11), 2727−2736.
(9) Lilge, L. Use of Ru Complexes as Photosensitizers in Photodynamic Therapy. *Ru Complexes*; John Wiley & Sons, Ltd., 2017; pp 117−137.
(10) Mari, C.; Pierroz, V.; Ferrari, S.; Gasser, G. Combination of Ru(II) Complexes and Light: New Frontiers in Cancer Therapy. *Chem. Sci.* **2015**, *6* (5), 2660−2686.
(11) Monro, S.; Colón, K. L.; Yin, H.; Roque, J.; Konda, P.; Gujar, S.; Thummel, R. P.; Lilge, L.; Cameron, C. G.; McFarland, S. A. Transition Metal Complexes and Photodynamic Therapy from a Tumor-Centered Approach: Challenges, Opportunities, and Highlights from the Development of TLD1433. *Chem. Rev.* **2019**, *119* (2), 797−828.
(12) Liu, J.; Zhang, C.; Rees, T. W.; Ke, L.; Ji, L.; Chao, H. Harnessing Ru(II) as Photodynamic Agents: Encouraging Advances in Cancer Therapy. *Coord. Chem. Rev.* **2018**, *363*, 17−28.
(13) Dickerson, M.; Sun, Y.; Howerton, B.; Glazer, E. C. Modifying Charge and Hydrophilicity of Simple Ru(II) Polypyridyl Complexes Radically Alters Biological Activities: Old Complexes, Surprising New Tricks. *Inorg. Chem.* **2014**, *53* (19), 10370−10377.
(14) Liu, Y.; Hammitt, R.; Lutterman, D. A.; Joyce, L. E.; Thummel, R. P.; Turro, C. Ru(II) Complexes of New Tridentate Ligands: Unexpected High Yield of Sensitized 1O2. *Inorg. Chem.* **2009**, *48* (1), 375−385.
(15) Meijer, M. S.; Carlos, R. M.; Baptista, M. S.; Bonnet, S. Photomedicine with Inorganic Complexes: A Bright Future. In *Springer Handbook of Inorganic Photochemistry*; Bahnemann, D.; Patrocinio, A. O. T., Eds.; Springer International Publishing: Cham, 2022; pp 1015−1033.
(16) Gill, M. R.; Thomas, J. A. Ru(II) Polypyridyl Complexes and DNA—from Structural Probes to Cellular Imaging and Therapeutics. *Chem. Soc. Rev.* **2012**, *41* (8), 3179−3192.
(17) Conti, L.; Macedi, E.; Giorgi, C.; Valtancoli, B.; Fusi, V. Combination of Light and Ru(II) Polypyridyl Complexes: Recent Advances in the Development of New Anticancer Drugs. *Coord. Chem. Rev.* **2022**, *469*, No. 214656.
(18) Karges, J. Clinical Development of Metal Complexes as Photosensitizers for Photodynamic Therapy of Cancer. *Angew. Chem., Int. Ed.* **2022**, *61* (5), No. e202112236.
(19) McFarland, S. A.; Mandel, A.; Dumoulin-White, R.; Gasser, G. Metal-Based Photosensitizers for Photodynamic Therapy: The Future of Multimodal Oncology. *Curr. Opin. Chem. Biol.* **2020**, *56*, 23−27.
(20) Fong, J.; Kasimova, K.; Arenas, Y.; Kaspler, P.; Lazic, S.; Mandel, A.; Lilge, L. A Novel Class of Ru-Based Photosensitizers Effectively Kills in Vitro Cancer Cells and in Vivo Tumors. *Photochem. Photobiol. Sci.* **2015**, *14* (11), 2014−2023.
(21) Karges, J.; Blacque, O.; Goldner, P.; Chao, H.; Gasser, G. Towards Long Wavelength Absorbing Photodynamic Therapy Photosensitizers via the Extension of a [Ru(Bipy)3]2+ Core. *Eur. J. Inorg. Chem.* **2019**, *2019* (32), 3704−3712.
(22) Wilson, B. C.; Jeeves, W. P.; Lowe, D. M. In Vivo and Post Mortem Measurements of the Attenuation Spectra of Light in Mammalian Tissues. *Photochem. Photobiol.* **1985**, *42* (2), 153−162.
(23) Karges, J.; Heinemann, F.; Jakubaszek, M.; Maschietto, F.; Subecz, C.; Dotou, M.; Vinck, R.; Blacque, O.; Tharaud, M.; Goud, B.; Viñuelas-Zahinos, E.; Spingler, B.; Ciofini, I.; Gasser, G. Rationally Designed Long-Wavelength Absorbing Ru(II) Polypyridyl Complexes as Photosensitizers for Photodynamic Therapy. *J. Am. Chem. Soc.* **2020**, *142* (14), 6578−6587.
(24) Mazuryk, O.; Magiera, K.; Rys, B.; Suzenet, F.; Kieda, C.; Brindell, M. Multifaceted Interplay between Lipophilicity, Protein Interaction and Luminescence Parameters of Non-Intercalative Ru(II) Polypyridyl Complexes Controlling Cellular Imaging and Cytotoxic Properties. *JBIC, J. Biol. Inorg. Chem.* **2014**, *19* (8), 1305−1316.
(25) Wen, Y.; Schreiber, C. L.; Smith, B. D. Dual-Targeted Phototherapeutic Agents as Magic Bullets for Cancer. *Bioconjugate Chem.* **2020**, *31* (3), 474−482.
(26) Arias, J. L. Drug Targeting Strategies in Cancer Treatment: An Overview. *Mini-Rev. Med. Chem.* **2011**, *11* (1), 1−17.
(27) Bae, Y. H.; Park, K. Targeted Drug Delivery to Tumors: Myths, Reality and Possibility. *J. Controlled Release* **2011**, *153* (3), 198−205.
(28) Sachdeva, M. S. Drug Targeting Systems for Cancer Chemotherapy. *Expert Opin. Invest. Drugs* **1998**, *7* (11), 1849−1864.
(29) Martínez-Alonso, M.; Gasser, G. Ru Polypyridyl Complex-Containing Bioconjugates. *Coord. Chem. Rev.* **2021**, *434*, No. 213736.
(30) McKenzie, L. K.; Flamme, M.; Felder, P. S.; Karges, J.; Bonhomme, F.; Gandioso, A.; Malosse, C.; Gasser, G.; Hollenstein, M. A Ru−Oligonucleotide Bioconjugated Photosensitizing Aptamer for Cancer Cell Specific Photodynamic Therapy. *RSC Chem. Biol.* **2022**, *3* (1), 85−95.
(31) Karges, J.; Jakubaszek, M.; Mari, C.; Zarschler, K.; Goud, B.; Stephan, H.; Gasser, G. Synthesis and Characterization of an Epidermal Growth Factor Receptor-Selective RuII Polypyridyl−Nanobody Conjugate as a Photosensitizer for Photodynamic Therapy. *ChemBioChem* **2020**, *21* (4), 531−542.
(32) Martínez-Alonso, M.; Gandioso, A.; Thibaudeau, C.; Qin, X.; Arnoux, P.; Demeubayeva, N.; Guérineau, V.; Frochot, C.; Jung, A. C.; Gaiddon, C.; Gasser, G. A Novel Near-IR Absorbing Ru(II) Complex as Photosensitizer for Photodynamic Therapy and Its Cetuximab Bioconjugates. *ChemBioChem* **2023**, *24*, No. e202300203, DOI: 10.1002/cbic.202300203.
(33) Huang, Y.; Huang, W.; Chan, L.; Zhou, B.; Chen, T. A Multifunctional DNA Origami as Carrier of Metal Complexes to Achieve Enhanced Tumoral Delivery and Nullified Systemic Toxicity. *Biomaterials* **2016**, *103*, 183−196.
(34) Zhu, X.; Zhou, H.; Liu, Y.; Wen, Y.; Wei, C.; Yu, Q.; Liu, J. Transferrin/Aptamer Conjugated Mesoporous Ru Nanosystem for Redox-Controlled and Targeted Chemo-Photodynamic Therapy of Glioma. *Acta Biomater.* **2018**, *82*, 143−157.
(35) Mari, C.; Pierroz, V.; Leonidova, A.; Ferrari, S.; Gasser, G. Towards Selective Light-Activated Ru^{II}-Based Prodrug Candidates: Towards Selective Light-Activated Ru^{II} -Based Prodrug Candidates. *Eur. J. Inorg. Chem.* **2015**, *2015* (23), 3879−3891.
(36) Joshi, T.; Pierroz, V.; Ferrari, S.; Gasser, G. Bis-(Dipyridophenazine)(2-(2′-Pyridyl)Pyrimidine-4-Carboxylic Acid)-Ru(II) Hexafluorophosphate: A Lesson in Stubbornness. *ChemMedChem* **2014**, *9* (7), 1419−1427.
(37) Silva, M. J. S. A.; Vinck, R.; Wang, Y.; Saubaméa, B.; Tharaud, M.; Dominguez-Jurado, E.; Karges, J.; Gois, P. M. P.; Gasser, G. Towards Selective Delivery of a Ru(II) Polypyridyl Complex-Containing Bombesin Conjugate into Cancer Cells. *ChemBioChem* **2023**, *24* (4), No. e202200647.
(38) Chan, L.; Huang, Y.; Chen, T. Cancer-Targeted Tri-Block Copolymer Nanoparticles as Payloads of Metal Complexes to Achieve Enhanced Cancer Theranosis. *J. Mater. Chem. B* **2016**, *4* (26), 4517−4525.
(39) Paul, S.; Kundu, P.; Bhattacharyya, U.; Garai, A.; Maji, R. C.; Kondaiah, P.; Chakravarty, A. R. Ru(II) Conjugates of Boron-Dipyrromethene and Biotin for Targeted Photodynamic Therapy in Red Light. *Inorg. Chem.* **2020**, *59* (1), 913−924.
(40) Vinck, R.; Gandioso, A.; Burckel, P.; Saubaméa, B.; Cariou, K.; Gasser, G. Red-Absorbing Ru(II) Polypyridyl Complexes with Biotin Targeting Spontaneously Assemble into Nanoparticles in Biological Media. *Inorg. Chem.* **2022**, *61* (34), 13576−13585.
(41) Li, J.; Zeng, L.; Xiong, K.; Rees, T. W.; Jin, C.; Wu, W.; Chen, Y.; Ji, L.; Chao, H. A Biotinylated Ru(II) Photosensitizer for Tumor-Targeted Two-Photon Photodynamic Therapy. *Chem. Commun.* **2019**, *55* (73), 10972−10975.
(42) Xiang, H.-J.; Deng, Q.; An, L.; Guo, M.; Yang, S.-P.; Liu, J.-G. Tumor Cell Specific and Lysosome-Targeted Delivery of Nitric Oxide for Enhanced Photodynamic Therapy Triggered by 808 Nm near-Infrared Light. *Chem. Commun.* **2016**, *52* (1), 148−151.

(43) Wang, T.; Zabarska, N.; Wu, Y.; Lamla, M.; Fischer, S.; Monczak, K.; Ng, D. Y. W.; Rau, S.; Weil, T. Receptor Selective Ru-Somatostatin Photosensitizer for Cancer Targeted Photodynamic Applications. *Chem. Commun.* **2015**, *51* (63), 12552−12555.
(44) Lameijer, L. N.; Hopkins, S. L.; Brevé, T. G.; Askes, S. H. C.; Bonnet, S. L-Glucose versus D-Glucose Conjugation: Mitochondrial Targeting of a Light-Activated Dual-Mode-of-Action Ru-Based Anticancer Prodrug. *Chem.—Eur. J.* **2016**, *22* (51), 18484−18491.
(45) Knežević, N. Ž.; Stojanovic, V.; Chaix, A.; Bouffard, E.; Cheikh, K. E.; Morère, A.; Maynadier, M.; Lemercier, G.; Garcia, M.; Gary-Bobo, M.; Durand, J.-O.; Cunin, F. Ru(II) Complex-Photosensitized Multifunctionalized Porous Silicon Nanoparticles for Two-Photon near-Infrared Light Responsive Imaging and Photodynamic Cancer Therapy. *J. Mater. Chem. B* **2016**, *4* (7), 1337−1342.
(46) Zhao, X.; Li, M.; Sun, W.; Fan, J.; Du, J.; Peng, X. An Estrogen Receptor Targeted Ru Complex as a Two-Photon Photodynamic Therapy Agent for Breast Cancer Cells. *Chem. Commun.* **2018**, *54* (51), 7038−7041.
(47) Jakubaszek, M.; Rossier, J.; Karges, J.; Delasoie, J.; Goud, B.; Gasser, G.; Zobi, F. Evaluation of the Potential of Cobalamin Derivatives Bearing Ru(II) Polypyridyl Complexes as Photosensitizers for Photodynamic Therapy. *Helv. Chim. Acta* **2019**, *102* (7), No. e1900104.
(48) Du, E.; Hu, X.; Roy, S.; Wang, P.; Deasy, K.; Mochizuki, T.; Zhang, Y. Taurine-Modified Ru(II)-Complex Targets Cancerous Brain Cells for Photodynamic Therapy. *Chem. Commun.* **2017**, *53* (44), 6033−6036.
(49) Fu, H.-G.; Chen, Y.; Yu, Q.; Liu, Y. A Tumor-Targeting Ru/Polysaccharide/Protein Supramolecular Assembly with High Photodynamic Therapy Ability. *Chem. Commun.* **2019**, *55* (21), 3148−3151.
(50) Kaspler, P.; Lazic, S.; Forward, S.; Arenas, Y.; Mandel, A.; Lilge, L. A Ru(II) Based Photosensitizer and Transferrin Complexes Enhance Photo-Physical Properties, Cell Uptake, and Photodynamic Therapy Safety and Efficacy. *Photochem. Photobiol. Sci.* **2016**, *15* (4), 481−495.
(51) Dickerson, M.; Howerton, B.; Bae, Y.; Glazer, E. C. Light-Sensitive Ru Complex-Loaded Cross-Linked Polymeric Nanoassemblies for the Treatment of Cancer. *J. Mater. Chem. B* **2016**, *4* (3), 394−408.
(52) Appold, M.; Mari, C.; Lederle, C.; Elbert, J.; Schmidt, C.; Ott, I.; Stühn, B.; Gasser, G.; Gallei, M. Multi-Stimuli Responsive Block Copolymers as a Smart Release Platform for a Polypyridyl Ru Complex. *Polym. Chem.* **2017**, *8* (5), 890−900.
(53) Sun, W.; Li, S.; Häupler, B.; Liu, J.; Jin, S.; Steffen, W.; Schubert, U. S.; Butt, H.-J.; Liang, X.-J.; Wu, S. An Amphiphilic Ru Polymetallodrug for Combined Photodynamic Therapy and Photochemotherapy In Vivo. *Adv. Mater.* **2017**, *29* (6), No. 1603702.
(54) Sun, W.; Parowatkin, M.; Steffen, W.; Butt, H.-J.; Mailänder, V.; Wu, S. Ru-Containing Block Copolymer Assemblies: Red-Light-Responsive Metallopolymers with Tunable Nanostructures for Enhanced Cellular Uptake and Anticancer Phototherapy. *Adv. Healthcare Mater.* **2016**, *5* (4), 467−473.
(55) Boeuf, G.; Roullin, G. V.; Moreau, J.; Van Gulick, L.; Zambrano Pineda, N.; Terryn, C.; Ploton, D.; Andry, M. C.; Chuburu, F.; Dukic, S.; Molinari, M.; Lemercier, G. Encapsulated Ru(II) Complexes in Biocompatible Poly(d,l-Lactide-Co-Glycolide) Nanoparticles for Application in Photodynamic Therapy. *ChemPlusChem* **2014**, *79* (1), 171−180.
(56) Moreno, M. J.; Monson, E.; Reddy, R. G.; Rehemtulla, A.; Ross, B. D.; Philbert, M.; Schneider, R. J.; Kopelman, R. Production of Singlet Oxygen by Ru(Dpp(SO3)2)3 Incorporated in Polyacrylamide PEBBLES. *Sens. Actuators, B* **2003**, *90* (1−3), 82−89.
(57) Soliman, N.; McKenzie, L. K.; Karges, J.; Bertrand, E.; Tharaud, M.; Jakubaszek, M.; Guérineau, V.; Goud, B.; Hollenstein, M.; Gasser, G.; Thomas, C. M. Ru-Initiated Polymerization of Lactide: A Route to Remarkable Cellular Uptake for Photodynamic Therapy of Cancer. *Chem. Sci.* **2020**, *11* (10), 2657−2663.
(58) Karges, J.; Li, J.; Zeng, L.; Chao, H.; Gasser, G. Polymeric Encapsulation of a Ru Polypyridine Complex for Tumor Targeted One- and Two-Photon Photodynamic Therapy. *ACS Appl. Mater. Interfaces* **2020**, *12* (49), 54433−54444.
(59) Askes, S.; Meijer, M.; Bouwens, T.; Landman, I.; Bonnet, S. Red Light Activation of Ru(II) Polypyridyl Prodrugs via Triplet-Triplet Annihilation Upconversion: Feasibility in Air and through Meat. *Molecules* **2016**, *21* (11), No. 1460, DOI: 10.3390/molecules21111460.
(60) Maranho, D. S.; de Lima, R. G.; Primo, F. L.; da Silva, R. S.; Tedesco, A. C. Photoinduced Nitric Oxide and Singlet Oxygen Release from ZnPC Liposome Vehicle Associated with the Nitrosyl Ru Complex: Synergistic Effects in Photodynamic Therapy Application. *Photochem. Photobiol.* **2009**, *85* (3), 705−713.
(61) Wang, N.; Feng, Y.; Zeng, L.; Zhao, Z.; Chen, T. Functionalized Multiwalled Carbon Nanotubes as Carriers of Ru Complexes to Antagonize Cancer Multidrug Resistance and Radioresistance. *ACS Appl. Mater. Interfaces* **2015**, *7* (27), 14933−14945.
(62) Zhang, P.; Huang, H.; Huang, J.; Chen, H.; Wang, J.; Qiu, K.; Zhao, D.; Ji, L.; Chao, H. Noncovalent Ru(II) Complexes−Single-Walled Carbon Nanotube Composites for Bimodal Photothermal and Photodynamic Therapy with Near-Infrared Irradiation. *ACS Appl. Mater. Interfaces* **2015**, *7* (41), 23278−23290.
(63) Zhang, D.-Y.; Zheng, Y.; Tan, C.-P.; Sun, J.-H.; Zhang, W.; Ji, L.-N.; Mao, Z.-W. Graphene Oxide Decorated with Ru(II)−Polyethylene Glycol Complex for Lysosome-Targeted Imaging and Photodynamic/Photothermal Therapy. *ACS Appl. Mater. Interfaces* **2017**, *9* (8), 6761−6771.
(64) Zhang, W.; Li, B.; Ma, H.; Zhang, L.; Guan, Y.; Zhang, Y.; Zhang, X.; Jing, P.; Yue, S. Combining Ru(II) Complexes with Metal−Organic Frameworks to Realize Effective Two-Photon Absorption for Singlet Oxygen Generation. *ACS Appl. Mater. Interfaces* **2016**, *8* (33), 21465−21471.
(65) Chen, R.; Zhang, J.; Chelora, J.; Xiong, Y.; Kershaw, S. V.; Li, K. F.; Lo, P.-K.; Cheah, K. W.; Rogach, A. L.; Zapien, J. A.; Lee, C.-S. Ru(II) Complex Incorporated UiO-67 Metal−Organic Framework Nanoparticles for Enhanced Two-Photon Fluorescence Imaging and Photodynamic Cancer Therapy. *ACS Appl. Mater. Interfaces* **2017**, *9* (7), 5699−5708.
(66) Ruggiero, E.; Garino, C.; Mareque-Rivas, J. C.; Habtemariam, A.; Salassa, L. Upconverting Nanoparticles Prompt Remote Near-Infrared Photoactivation of Ru(II)-Arene Complexes. *Chem.—Eur. J.* **2016**, *22* (8), 2801−2811.
(67) Moreau, J.; Lux, F.; Four, M.; Olesiak-Banska, J.; Matczyszyn, K.; Perriat, P.; Frochot, C.; Arnoux, P.; Tillement, O.; Samoc, M.; Ponterini, G.; Roux, S.; Lemercier, G. A 5-(Difluorenyl)-1,10-Phenanthroline-Based Ru(II) Complex as a Coating Agent for Potential Multifunctional Gold Nanoparticles. *Phys. Chem. Chem. Phys.* **2014**, *16* (28), 14826−14833.
(68) Ricciardi, L.; Martini, M.; Tillement, O.; Sancey, L.; Perriat, P.; Ghedini, M.; Szerb, E. I.; Yadav, Y. J.; La Deda, M. Multifunctional Material Based on Ionic Transition Metal Complexes and Gold−Silica Nanoparticles: Synthesis and Photophysical Characterization for Application in Imaging and Therapy. *J. Photochem. Photobiol., B* **2014**, *140*, 396−404.
(69) Zhou, Z.; Liu, J.; Huang, J.; Rees, T. W.; Wang, Y.; Wang, H.; Li, X.; Chao, H.; Stang, P. J. A Self-Assembled Ru−Pt Metallacage as a Lysosome-Targeting Photosensitizer for 2-Photon Photodynamic Therapy. *Proc. Natl. Acad. Sci. U.S.A.* **2019**, *116* (41), 20296−20302.
(70) Meijer, M. S.; Talens, V. S.; Hilbers, M. F.; Kieltyka, R. E.; Brouwer, A. M.; Natile, M. M.; Bonnet, S. NIR-Light-Driven Generation of Reactive Oxygen Species Using Ru(II)-Decorated Lipid-Encapsulated Upconverting Nanoparticles. *Langmuir* **2019**, *35* (37), 12079−12090.
(71) Shi, H.; Fang, T.; Tian, Y.; Huang, H.; Liu, Y. A Dual-Fluorescent Nano-Carrier for Delivering Photoactive Ru Polypyridyl Complexes. *J. Mater. Chem. B* **2016**, *4* (27), 4746−4753.
(72) Ellahioui, Y.; Patra, M.; Mari, C.; Kaabi, R.; Karges, J.; Gasser, G.; Gómez-Ruiz, S. Mesoporous Silica Nanoparticles Functionalised

with a Photoactive Ru(II) Complex: Exploring the Formulation of a Metal-Based Photodynamic Therapy Photosensitiser. *Dalton Trans.* **2019**, *48* (18), 5940−5951.
(73) Chakrabortty, S.; Agrawalla, B. K.; Stumper, A.; Vegi, N. M.; Fischer, S.; Reichardt, C.; Kögler, M.; Dietzek, B.; Feuring-Buske, M.; Buske, C.; Rau, S.; Weil, T. Mitochondria Targeted Protein-Ru Photosensitizer for Efficient Photodynamic Applications. *J. Am. Chem. Soc.* **2017**, *139* (6), 2512−2519.
(74) Arora, K.; Herroon, M.; Al-Afyouni, M. H.; Toupin, N. P.; Rohrabaugh, T. N.; Loftus, L. M.; Podgorski, I.; Turro, C.; Kodanko, J. J. Catch and Release Photosensitizers: Combining Dual-Action Ru Complexes with Protease Inactivation for Targeting Invasive Cancers. *J. Am. Chem. Soc.* **2018**, *140* (43), 14367−14380.
(75) Hally, C.; Delcanale, P.; Nonell, S.; Viappiani, C.; Abbruzzetti, S. Photosensitizing Proteins for Antibacterial Photodynamic Inactivation. *Transl. Biophotonics* **2020**, *2* (1−2), No. e201900031.
(76) Hoogenboezem, E. N.; Duvall, C. L. Harnessing Albumin as a Carrier for Cancer Therapies. *Adv. Drug Delivery Rev.* **2018**, *130*, 73−89.
(77) Peters, T. Serum Albumin. *Advances in Protein Chemistry*; Academic Press Inc., 1985; Vol. 37, pp 161−245.
(78) Matsumura, Y.; Maeda, H. A New Concept for Macromolecular Therapeutics in Cancer Chemotherapy: Mechanism of Tumoritropic Accumulation of Proteins and the Antitumor Agent Smancs. *Cancer Res.* **1986**, *46* (12 Pt 1), 6387−6392.
(79) Maeda, H. The Enhanced Permeability and Retention (EPR) Effect in Tumor Vasculature: The Key Role of Tumor-Selective Macromolecular Drug Targeting. *Adv. Enzyme Regul.* **2001**, *41* (1), 189−207.
(80) Maeda, H.; Wu, J.; Sawa, T.; Matsumura, Y.; Hori, K. Tumor Vascular Permeability and the EPR Effect in Macromolecular Therapeutics: A Review. *J. Controlled Release* **2000**, *65* (1−2), 271−284.
(81) Desai, N.; Trieu, V.; Yao, Z.; Louie, L.; Ci, S.; Yang, A.; Tao, C.; De, T.; Beals, B.; Dykes, D.; Noker, P.; Yao, R.; Labao, E.; Hawkins, M.; Soon-Shiong, P. Increased Antitumor Activity, Intratumor Paclitaxel Concentrations, and Endothelial Cell Transport of Cremophor-Free, Albumin-Bound Paclitaxel, ABI-007, Compared with Cremophor-Based Paclitaxel. *Clin. Cancer Res.* **2006**, *12* (4), 1317−1324.
(82) John, T. A.; Vogel, S. M.; Tiruppathi, C.; Malik, A. B.; Minshall, R. D. Quantitative Analysis of Albumin Uptake and Transport in the Rat Microvessel Endothelial Monolayer. *Am. J. Physiol.: Lung Cell. Mol. Physiol.* **2003**, *284* (1), L187−L196.
(83) Gradishar, W. J.; Tjulandin, S.; Davidson, N.; Shaw, H.; Desai, N.; Bhar, P.; Hawkins, M.; O'Shaughnessy, J. Phase III Trial of Nanoparticle Albumin-Bound Paclitaxel Compared with Polyethylated Castor Oil-Based Paclitaxel in Women with Breast Cancer. *J. Clin. Oncol.* **2005**, *23* (31), 7794−7803.
(84) Stinchcombe, T. E. Nanoparticle Albumin-Bound Paclitaxel: A Novel Cremphor-EL-Free Formulation of Paclitaxel. *Nanomedicine* **2007**, *2* (4), 415−423.
(85) Abraxane_Product_Monograph_English_Version.Pdf, 2020. https://media.celgene.com/content/uploads/sites/23/Abraxane_Product_Monograph_English_Version.pdf (accessed March 27, 2020).
(86) Dömötör, O.; Pivarcsik, T.; Mészáros, J. P.; Szatmári, I.; Fülöp, F.; Enyedy, É. A. Critical Factors Affecting the Albumin Binding of Half-Sandwich Ru(II) and Rh(III) Complexes of 8-Hydroxyquinolines and Oligopyridines. *Dalton Trans.* **2021**, *50* (34), 11918−11930.
(87) Laznicwska, J.; Agostino, M.; Hickey, S. M.; Parkinson-Lawrence, E.; Stagni, S.; Massi, M.; Brooks, D. A.; Plush, S. E. Spectroscopic and Molecular Docking Study of the Interaction between Neutral Re(I) Tetrazolate Complexes and Bovine Serum Albumin. *Chem.—Eur. J.* **2021**, *27* (44), 11406−11417.
(88) Gou, Y.; Zhang, Y.; Yang, F.; Liang, H. Evaluation of Interactions Between Platinum-/Ru-Based Anticancer Agents and Human Serum Albumin: Development of HSA Carrier for Metal-Based Drugs. *Curr. Pharm. Des.* **2015**, *21* (14), 1848−1861.
(89) Gou, Y.; Qi, J.; Ajayi, J.-P.; Zhang, Y.; Zhou, Z.; Wu, X.; Yang, F.; Liang, H. Developing Anticancer Copper(II) Pro-Drugs Based on the Nature of Cancer Cells and the Human Serum Albumin Carrier IIA Subdomain. *Mol. Pharmaceutics* **2015**, *12* (10), 3597−3609.
(90) Kozsup, M.; Dömötör, O.; Nagy, S.; Farkas, E.; Enyedy, É. A.; Buglyó, P. Synthesis, Characterization and Albumin Binding Capabilities of Quinizarin Containing Ternary Cobalt(III) Complexes. *J. Inorg. Biochem.* **2020**, *204*, No. 110963.
(91) Kratz, F. Albumin as a Drug Carrier: Design of Prodrugs, Drug Conjugates and Nanoparticles. *J. Controlled Release* **2008**, *132* (3), 171−183.
(92) Elsadek, B.; Kratz, F. Impact of Albumin on Drug Delivery–New Applications on the Horizon. *J. Controlled Release* **2012**, *157* (1), 4−28.
(93) Fronik, P.; Gutmann, M.; Vician, P.; Stojanovic, M.; Kastner, A.; Heffeter, P.; Pirker, C.; Keppler, B. K.; Berger, W.; Kowol, C. R. A Platinum(IV) Prodrug Strategy to Overcome Glutathione-Based Oxaliplatin Resistance. *Commun. Chem.* **2022**, *5* (1), No. 46, DOI: 10.1038/s42004-022-00661-z.
(94) Schueffl, H.; Theiner, S.; Hermann, G.; Mayr, J.; Fronik, P.; Groza, D.; van Schonhooven, S.; Galvez, L.; Sommerfeld, N. S.; Schintlmeister, A.; Reipert, S.; Wagner, M.; Mader, R. M.; Koellensperger, G.; Keppler, B. K.; Berger, W.; Kowol, C. R.; Legin, A.; Heffeter, P. Albumin-Targeting of an Oxaliplatin-Releasing Platinum(IV) Prodrug Results in Pronounced Anticancer Activity Due to Endocytotic Drug Uptake in Vivo. *Chem. Sci.* **2021**, *12* (38), 12587−12599.
(95) Fronik, P.; Poetsch, I.; Kastner, A.; Mendrina, T.; Hager, S.; Hohenwallner, K.; Schueffl, H.; Herndler-Brandstetter, D.; Koellensperger, G.; Rampler, E.; Kopecka, J.; Riganti, C.; Berger, W.; Keppler, B. K.; Heffeter, P.; Kowol, C. R. Structure−Activity Relationships of Triple-Action Platinum(IV) Prodrugs with Albumin-Binding Properties and Immunomodulating Ligands. *J. Med. Chem.* **2021**, *64* (16), 12132−12151.
(96) Warnecke, A.; Fichtner, I.; Garmann, D.; Jaehde, U.; Kratz, F. Synthesis and Biological Activity of Water-Soluble Maleimide Derivatives of the Anticancer Drug Carboplatin Designed as Albumin-Binding Prodrugs. *Bioconjugate Chem.* **2004**, *15* (6), 1349−1359.
(97) Hanif, M.; Nazarov, A. A.; Legin, A.; Groessl, M.; Arion, V. B.; Jakupec, M. A.; Tsybin, Y. O.; Dyson, P. J.; Keppler, B. K.; Hartinger, C. G. Maleimide-Functionalised OrganoRu Anticancer Agents and Their Binding to Thiol-Containing Biomolecules. *Chem. Commun.* **2012**, *48* (10), 1475−1477.
(98) Hanif, M.; Moon, S.; Sullivan, M. P.; Movassaghi, S.; Kubanik, M.; Goldstone, D. C.; Söhnel, T.; Jamieson, S. M. F.; Hartinger, C. G. Anticancer Activity of Ru- and Os(Arene) Compounds of a Maleimide-Functionalized Bioactive Pyridinecarbothioamide Ligand. *J. Inorg. Biochem.* **2016**, *165*, 100−107.
(99) Moon, S.; Hanif, M.; Kubanik, M.; Holtkamp, H.; Söhnel, T.; Jamieson, S. M. F.; Hartinger, C. G. OrganoRu and Osmium Anticancer Complexes Bearing a Maleimide Functional Group: Reactivity to Cysteine, Stability, and Cytotoxicity. *ChemPlusChem* **2015**, *80* (1), 231−236.
(100) Pichler, V.; Mayr, J.; Heffeter, P.; Dömötör, O.; Enyedy, É. A.; Hermann, G.; Groza, D.; Köllensperger, G.; Galanksi, M.; Berger, W.; Keppler, B. K.; Kowol, C. R. Maleimide-Functionalised Platinum(IV) Complexes as a Synthetic Platform for Targeted Drug Delivery. *Chem. Commun.* **2013**, *49* (22), 2249−2251.
(101) Panetta, C. A.; Kumpaty, H. J.; Heimer, N. E.; Leavy, M. C.; Hussey, C. L. Disulfide-Functionalized 3-, 4-, 5-, and 6-Substituted 2,2′-Bipyridines and Their Ru Complexes. *J. Org. Chem.* **1999**, *64* (3), 1015−1021.
(102) Sullivan, B. P.; Salmon, D. J.; Meyer, T. J. Mixed Phosphine 2,2′-Bipyridine Complexes of Ru. *Inorg. Chem.* **1978**, *17* (12), 3334−3341.
(103) Nakagawa, A.; Ito, A.; Sakuda, E.; Fujii, S.; Kitamura, N. Emission Tuning of Heteroleptic Arylborane−Ru(II) Complexes by

Ancillary Ligands: Observation of Strickler−Berg-Type Relation. *Inorg. Chem.* **2018**, *57* (15), 9055−9066.
(104) Shinchi, H.; Komaki, F.; Yuki, M.; Ohara, H.; Hayakawa, N.; Wakao, M.; Cottam, H. B.; Hayashi, T.; Carson, D. A.; Moroishi, T.; Suda, Y. Glyco-Nanoadjuvants: Impact of Linker Length for Conjugating a Synthetic Small-Molecule TLR7 Ligand to Glyco-Nanoparticles on Immunostimulatory Effects. *ACS Chem. Biol.* **2022**, *17* (4), 957−968.
(105) Singh, S.; Oyagawa, C. R. M.; Macdonald, C.; Grimsey, N. L.; Glass, M.; Vernall, A. J. Chromenopyrazole-Based High Affinity, Selective Fluorescent Ligands for Cannabinoid Type 2 Receptor. *ACS Med. Chem. Lett.* **2019**, *10* (2), 209−214.
(106) Matsui, S.; Aida, H. Hydrolysis of Some N-Alkylmaleimides. *J. Chem. Soc., Perkin Trans. 2* **1978**, *12*, 1277−1280.
(107) Gregory, J. D. The Stability of N-Ethylmaleimide and Its Reaction with Sulfhydryl Groups. *J. Am. Chem. Soc.* **1955**, *77* (14), 3922−3923.
(108) Chen, X.; Murawski, A.; Patel, K.; Crespi, C. L.; Balimane, P. V. A Novel Design of Artificial Membrane for Improving the PAMPA Model. *Pharm. Res.* **2008**, *25* (7), 1511−1520.
(109) Luo, Z.; Yu, L.; Yang, F.; Zhao, Z.; Yu, B.; Lai, H.; Wong, K.-H.; Ngai, S.-M.; Zheng, W.; Chen, T. Ru Polypyridyl Complexes as Inducer of ROS-Mediated Apoptosis in Cancer Cells by Targeting Thioredoxin Reductase. *Metallomics* **2014**, *6* (8), 1480−1490.
(110) Alatrash, N.; Narh, E. S.; Yadav, A.; Kim, M.-J.; Janaratne, T.; Gabriel, J.; MacDonnell, F. M. Synthesis, DNA Cleavage Activity, Cytotoxicity, Acetylcholinesterase Inhibition, and Acute Murine Toxicity of Redox-Active Ru(II) Polypyridyl Complexes. *ChemMedChem* **2017**, *12* (13), 1055−1069.
(111) Zava, O.; Zakeeruddin, S. M.; Danelon, C.; Vogel, H.; Grätzel, M.; Dyson, P. J. A Cytotoxic Ru Tris(Bipyridyl) Complex That Accumulates at Plasma Membranes. *ChemBioChem* **2009**, *10* (11), 1796−1800.
(112) Lakowicz, J. R. *Principles of Fluorescence Spectroscopy*, 3rd ed.; Springer US, 2006.
(113) Oettl, K.; Stauber, R. E. Physiological and Pathological Changes in the Redox State of Human Serum Albumin Critically Influence Its Binding Properties. *Br. J. Pharmacol.* **2007**, *151* (5), 580−590.
(114) Vinck, R.; Karges, J.; Tharaud, M.; Cariou, K.; Gasser, G. Physical, Spectroscopic, and Biological Properties of Ru and Osmium Photosensitizers Bearing Diversely Substituted 4,4′-Di(Styryl)-2,2′-Bipyridine Ligands. *Dalton Trans.* **2021**, *50* (41), 14629−14639.
(115) Wang, R.; Li, X.; Yoon, J. Organelle-Targeted Photosensitizers for Precision Photodynamic Therapy. *ACS Appl. Mater. Interfaces* **2021**, *13* (17), 19543−19571.
(116) Bernardim, B.; Cal, P. M. S. D.; Matos, M. J.; Oliveira, B. L.; Martínez-Sáez, N.; Albuquerque, I. S.; Perkins, E.; Corzana, F.; Burtoloso, A. C. B.; Jiménez-Osés, G.; Bernardes, G. J. L. Stoichiometric and Irreversible Cysteine-Selective Protein Modification Using Carbonylacrylic Reagents. *Nat. Commun.* **2016**, *7* (1), No. 13128.
(117) Ru Complexes. In *Inorganic Syntheses*; Rauchfuss, T. B., Ed.; John Wiley & Sons, Inc.: Hoboken, NJ, 2010; pp 148−163.
(118) Broomhead, J. A.; Young, C. G.; Hood, P. Tris(2,2″-Bipyridine)Ru(II) Dichloride Hexahydrate. *Inorganic Syntheses*; John Wiley & Sons, Ltd., 1990; pp 338−340.
(119) Dömötör, O.; Hartinger, C. G.; Bytzek, A. K.; Kiss, T.; Keppler, B. K.; Enyedy, E. A. Characterization of the Binding Sites of the Anticancer Ru(III) Complexes KP1019 and KP1339 on Human Serum Albumin via Competition Studies. *JBIC, J. Biol. Inorg. Chem.* **2013**, *18* (1), 9−17.
(120) Enyedy, É. A.; Hollender, D.; Kiss, T. Lipophilicity of Kinetically Labile Metal Complexes through the Example of Antidiabetic Zn(II) and VO(IV) Compounds. *J. Pharm. Biomed. Anal.* **2011**, *54* (5), 1073−1081.
(121) Gans, P.; Sabatini, A.; Vacca, A. Investigation of Equilibria in Solution. Determination of Equilibrium Constants with the HYPERQUAD Suite of Programs. *Talanta* **1996**, *43* (10), 1739−1753.
(122) Enyedy, É. A.; Dömötör, O.; Bali, K.; Hetényi, A.; Tuccinardi, T.; Keppler, B. K. Interaction of the Anticancer Gallium(III) Complexes of 8-Hydroxyquinoline and Maltol with Human Serum Proteins. *JBIC, J. Biol. Inorg. Chem.* **2015**, *20* (1), 77−88.

https://doi.org/10.1021/acs.inorgchem.3c01984
Inorg. Chem. 2023, 62, 15510−15526